Table 2
k_i values of each ROI in patients with schizophrenia and normal controls

Region	L/R	Controls	Patients	ANCOVA#	
		(n=20)	(n=18)	F	p
Parahippocampus	L	4.54±1.13	4.91±1.45	0.704	0.407
	R	4.76±1.11	4.47±1.29	0.528	0.472
Temporal cortex	L	1.92±0.99	1.98±0.81	0.041	0.842
	R	1.86±0.83	1.92±0.87	0.037	0.849
Prefrontal cortex	L	1.31±0.73	1.22±0.64	0.324	0.573
	R	1.35±0.73	1.35±0.57	0	1.000
Thalamus	L	3.55±1.60	3.19±1.72	0.549	0.463
	R	3.11±1.45	3.09±1.54	0.001	0.970
Putamen	L	15.52±2.04	15.76±2.14	0.139	0.711
	R	15.39±2.31	14.90±3.01	0.329	0.570
Caudate	L	12.89±2.68	14.66±2.38	4.409	0.043*
	R	13.71±2.74	13.59±2.09	0.026	0.872
Anterior cingulate	L	2.74±1.33	3.05±1.50	0.445	0.509
	R	3.24±1.73	3.00±1.13	0.288	0.595

Dopamine synthesis rates, expressed as $k_i \times 1000$, were presented as mean ± standard deviation.
#: Analysis of covariance with age as covariate (df= 1, 35).
L indicates left and R indicates right. The symbol * represents $p<0.05$.

2.3. Magnetic resonance images

For each participant, a structure magnetic resonance (MR) image was obtained. All MR imaging studies were performed with a 1.5-Tesla MR scanner (Philips Medical Systems, Best, The Netherlands). Three-dimensional volumetric acquisition of a T1-weighted gradient echo sequence produced a gapless series of thin transverse sections (echo time, TE: 9.2 ms; repetition time, TR: 21 ms; flip angle: 30°; field of view: 256 mm; acquisition matrix: 256×256; slice thickness: 1 mm).

2.4. Data analysis

All MR images were coregistered to the PET summation images of all frames using statistical parametric mapping 2 (SPM2; http://www.fil.ion.ucl.ac.uk/spm/software/spm2/). Regions of interest (ROIs) were drawn on the coregistered MR images, referring to the human brain atlas (Mai et al., 1997), and then transferred to the PET images. ROIs were defined for the prefrontal cortex, temporal cortex, anterior cingulate, parahippocampus, thalamus, caudate nucleus, and putamen. The ROIs were set on both left and right sides of the brain and those values were independently evaluated. To obtain regional time-activity curves, regional radioactivity was calculated for each frame, corrected for decay, and plotted versus time.

The overall uptake rate constant k_i of L-[β-^{11}C]DOPA, which indicates the net dopamine synthesis rate, was determined for each ROI by the graphical plot analysis method developed by Gjedde and Patlak (Gjedde, 1982; Ito et al., 2006; Patlak and Blasberg, 1985). k_i values can be estimated by simple linear least-squares fitting as follows:

$$\frac{C_i(t)}{C_i'(t)} = k_i \frac{\int_0^t C_i'(\tau)d\tau}{C_i'(t)} + F_{t>t^*}$$

where C_i is the total radioactivity concentration in a brain region that can be measured by PET, C_i' is the total radioactivity concentration in the reference brain region with no irreversible compartments, and t^* is the equilibrium time of the compartment for unchanged radioligand in the brain tissue. Plotting $C_i(t)/C_i'(t)$ versus $\int_0^t C_i'(\tau)d\tau/C_i'(t)$, after the time t^*, yields a straight line with the slope k_i and intercept F. In the present study, the occipital cortex was used as reference region (Ito et al., 2006). A range of equilibrium time t^* of 31.5 to 61.5 min was used.

ROI analyses were independently performed by 3 researchers who were blinded to the diagnoses. The intraclass correlation coefficient across all ROIs was 0.976 (McGraw and Wong, 1996), considered as excellent. In order to reduce variance, the k_i values by one researcher that most frequently showed medium values among those obtained by the 3 researchers were used for the following analyses.

2.5. Statistical analysis

Demographic variables were compared by independent sample t-test or chi-square test. Differences in the k_i values for each of the 7 × 2 brain regions between patients and controls were evaluated by one-way univariate analyses of covariance with age as a covariate, since an effect of age on k_i values has been reported (Ota et al., 2006). Pearson's correlation coefficients were calculated between the PANSS scores and k_i values. A significance level of $p<0.05$ (two-tailed) was used both in the comparison analyses between groups and in the correlation analyses.

3. Results

3.1. Demographic data

The demographic data of schizophrenia patients and controls are shown in Table 1. There were no significant differences between patients and controls in terms of age, gender, education, handedness, and the injected dose and

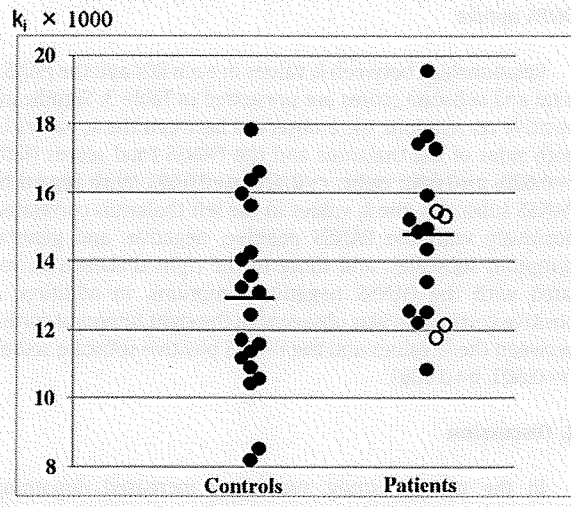

Fig. 1. Comparison of k_i values between patients with schizophrenia and control subjects in the left caudate nucleus. Horizontal lines represent mean values of the groups. Among patients, the closed circles indicate the values of antipsychotic drug-naïve patients, whereas the open circles indicate those of drug-free patients.

Table 3
Correlations between k_i values of each ROI and PANSS scores in schizophrenia

Region	L/R	Total scores		Positive symptoms		Negative symptoms		General symptoms	
		r	p	r	p	r	p	r	p
Parahippocampus	L	−0.003	0.992	0.045	0.859	0.080	0.752	−0.083	0.745
	R	0.284	0.253	0.288	0.246	0.197	0.434	0.245	0.328
Temporal cortex	L	−0.088	0.728	0.133	0.598	−0.049	0.848	−0.232	0.355
	R	0.465	0.052	0.603	0.008*	0.242	0.334	0.361	0.141
Prefrontal cortex	L	0.380	0.120	0.288	0.246	0.339	0.168	0.346	0.160
	R	0.407	0.094	0.302	0.082	0.457	0.057	0.320	0.196
Thalamus	L	0.620	0.006*	0.490	0.039*	0.504	0.033*	0.589	0.010*
	R	0.470	0.049*	0.378	0.122	0.492	0.038*	0.372	0.129
Putamen	L	0.247	0.323	0.177	0.482	0.342	0.165	0.160	0.525
	R	0.359	0.143	0.327	0.186	0.407	0.094	0.240	0.338
Caudate	L	0.287	0.323	0.294	0.236	0.319	0.197	0.174	0.490
	R	−0.183	0.468	−0.223	0.375	0.021	0.935	−0.220	0.380
Anterior cingulate	L	−0.270	0.120	0.202	0.421	−0.418	0.085	−0.412	0.089
	R	0.355	0.149	0.421	0.082	0.303	0.222	0.231	0.357

L indicates left and R indicates right.
The symbol * represents $p<0.05$.

specific radioactivity of L-[β-^{11}C]DOPA. The duration of illness and the PANSS scores are also shown in Table 1.

3.2. Regional L-[β-^{11}C]DOPA uptake in schizophrenia and control subjects

Univariate analysis of covariance revealed no significant interaction between group and age in any of the regions, and a significant group difference in k_i values only for the left caudate between normal controls and schizophrenia patients was observed (df=1, 35, F=4.409, p=0.043; Table 2 and Fig. 1). In addition, no significant difference was observed in the k_i values between antipsychotic drug-naïve and drug-free patients in any of the regions.

Furthermore, there was no significant correlation between the k_i values in any ROIs and the duration of illness in patients.

3.3. Severity of positive and negative symptoms and L-[β-^{11}C] DOPA uptake

Relationships between k_i values in each ROI and the PANSS total and subscale scores are presented in Table 3. Significant positive correlations were observed between the k_i values in both sides of the thalamus and the PANSS total scores (left: r=0.620, p=0.006; right: r=0.470, p=0.049). With regard to PANSS subscales, the k_i values in the left thalamus correlated positively with the PANSS positive, negative, and general symptom subscales, and those in the right thalamus correlated with the PANSS negative symptoms. In addition, a positive correlation was observed in the right temporal cortex between the k_i values and the PANSS positive subscale scores (r=0.603, p=0.008).

4. Discussion

In the present study, we found increased dopamine synthesis in the left caudate nucleus in patients with schizophrenia compared to normal controls. In addition, we observed a significant correlation between regional dopamine synthesis in the thalamus as well as in the right temporal cortex and symptom severity in patients.

Most of the previous studies with 6-[^{18}F]fluoro-L-DOPA have reported elevated dopamine synthesis mainly in the striatum of patients with schizophrenia (Hietala et al., 1995, 1999; McGowan et al., 2004; Reith et al., 1994), whereas decreased (Elkashef et al., 2000) or only greater variability (Dao-Castellana et al., 1997) have also been reported in this region. There are some plausible explanations for these inconsistent results. First, the participants with schizophrenia in these studies were not homogeneous. For example, one study investigated heterogeneous patients with psychosis (Reith et al., 1994), while the other studies included patients with schizoaffective disorder (Hietala et al., 1995, 1999). Furthermore, schizophrenia patients on antipsychotic medication participated in two of the PET studies (Elkashef et al., 2000; McGowan et al., 2004). Interestingly, a study on only unmedicated schizophrenia patients showed only greater variability in k_i values compared with normal controls (Dao-Castellana et al., 1997). Second, the differences between 6-[^{18}F] fluoro-L-DOPA and L-[β-^{11}C]DOPA in terms of 3-O-methyl metabolite of L-DOPA crossing the BBB might also result in such inconsistency (Ito et al., 2006; Melega et al., 1990; Torstenson et al., 1999). Kumakura et al. reported a method to reduce this problem with metabolites and demonstrated that catabolism and elimination of 6-[^{18}F]fluoro-L-DOPA was elevated nearly 2-fold in the striatum in 8 patients with schizophrenia as compared to that in 15 age-matched control subjects. They concluded that not only the synthesis but also the turnover of radiolabeled dopamine was increased in patients with schizophrenia (Kumakura et al., 2007).

Lindström et al. (1999) investigated unmedicated schizophrenia patients using L-[β-^{11}C]DOPA and found increased dopamine synthesis in the striatum and medial prefrontal cortex, while we observed elevated dopamine synthesis only in the left caudate. As for differences between the two studies, however, the patients in the study of Lindström et al. had relatively more severe psychotic symptoms (Clinical Global Impression ≥4) than our patients. In addition, our patients were mostly outpatients, and thus, such a difference in the demographic of patients might be responsible for the difference in results. In addition, the caudate nucleus might be more important than the putamen in the pathophysiology

of schizophrenia because the caudate has extensive interconnections from the limbic and cortical areas, which play crucial roles in the regulation of cognition and emotion compared to the putamen (Parent, 1990). Further, lateralization to the left of the caudate is consistent with the reports by Hietala et al. (1995, 1999).

With regard to the relationships with symptoms, in our patients, presynaptic dopamine synthesis in the thalamus was positively correlated with overall symptom severity, although that in the right thalamus was correlated only with PANSS negative scores, besides the PANSS total scores; in addition, dopamine synthesis in the right temporal cortex was positively correlated with positive symptoms. The thalamus has been repeatedly reported to be engaged in the pathophysiology of schizophrenia (Clinton and Meador-Woodruff, 2004; Takahashi et al., 2006). Previous neuroimaging studies have shown altered thalamic perfusion and metabolism (Andreasen et al., 1997; Buchsbaum et al., 1996; Clark et al., 2001; Hazlett et al., 1999, 2004; Kim et al., 2000; Mitelman et al., 2005; Resnick et al., 1988) and decreased dopamine D_2 receptor availability in the thalamus in patients with schizophrenia (Buchsbaum et al., 2006; Talvik et al., 2003, 2006; Yasuno et al., 2004). The thalamus is reported to have a pivotal role in the processing and integrating of sensory information related to emotional and cognitive functions (Clinton and Meador-Woodruff, 2004), and it has also been suggested to have sensory gating function (Carlsson et al., 2000; Takahashi et al., 2006). Further, elevated dopamine transmission in the thalamus was reported to disrupt sensory gating function (Young et al., 1995). Impaired gating function could contribute to both positive and negative symptoms by the inability to automatically "gate out" much redundant and unessential information, leading to irrelevant thought and fragmentation of mind and behavior in schizophrenia (Braff et al., 1999). Additionally, one study with 6-[^{18}F]fluoro-L-DOPA examined before and after 5 weeks of haloperidol treatment for schizophrenia demonstrated that the thalamus was the only structure in which the change of dopamine synthesis was related to improvement in negative symptoms (Gründer et al., 2003). Thus, dopaminergic regulation in the thalamus might be associated with positive and negative symptoms in schizophrenia. However, the contribution of different roles of each side of the thalamus to diverse symptom dimensions remains unclear.

In terms of the correlation between dopamine synthesis in the right temporal cortex and the PANSS scale, our data suggested that higher dopamine synthesis in the right temporal cortex might be associated with the expression of positive symptoms in patients with schizophrenia. Previous functional MRI studies have demonstrated the involvement of the right temporal cortex in some of the positive symptoms such as auditory hallucination (Shergill et al., 2000; Woodruff et al., 1997) and formal thought disorder (Kircher et al., 2002) in schizophrenia. On the other hand, although previous PET (Buchsbaum et al., 2006) and SPECT (Tuppurainen et al., 2003) studies have suggested decreased dopamine D_2R binding in the right temporal cortex, no significant correlation was found between the binding and positive symptoms. Furthermore, no study has demonstrated the relationship between presynaptic dopamine synthesis in the right temporal cortex and positive symptoms.

There are several limitations in the present study. First, smoking is regarded as a confounding factor in the estimation of k_i values (Salokangas et al., 2000), and some of our participants were smokers, although the smoking rate of the patients was only slightly higher than that of the normal controls (33% for patients and 20% for controls). Second, our patients consisted of both males and females, although we selected age- and gender-matched control subjects. Laakso et al. (2002) indicated gender differences in striatal dopamine synthesis with the use of 6-[^{18}F]fluoro-L-DOPA PET. However, we did not find such differences in our subjects (data not shown). Nonetheless, since gender differences have been suggested in schizophrenia (Salem and Kring, 1998), this issue should be addressed in future studies. Finally, although our sample size is hitherto the largest among reported studies on dopamine synthesis in schizophrenia, the current study may still not have enough power. Our results of both comparison and correlation analyses were significant only when uncorrected for multiple comparisons, and the failure to observe significant correlations with symptoms in other regions might be due to a type II error. Therefore, further investigations using still larger samples are required.

5. Conclusion

We measured the dopamine synthesis rate in patients with schizophrenia and normal control subjects by using PET with L-[β-^{11}C]DOPA. Patients had higher dopamine synthesis in the left caudate nucleus than controls, which was in line with the results of most previous studies that indicated an increase in dopamine synthesis in the striatum. Moreover, correlation analyses between k_i values and symptoms suggested that dopamine synthesis in the thalamus and right temporal cortex might be implicated in the pathophysiology of schizophrenia. There is little evidence concerning extrastriatal presynaptic dopaminergic functions of schizophrenia in vivo. Further studies are required to better understand the presynaptic dopaminergic functions of schizophrenia.

Role of funding source

This study was supported by a consignment expense for the Molecular Imaging Program on "Research Base for Exploring New Drugs" from the Ministry of Education, Culture, Sports, Science and Technology (MEXT), Japanese Government.

Contributors

S. Nozaki, F. Yasuno, A. Takano, and T. Suhara designed the study and wrote the protocol. S. Nozaki, M. Kato, F. Yasuno, M. Ota, A. Otsuka, and Y. Okubo recruited the patients and made psychiatric evaluations. S. Nozaki, H. Takano, M. Okumura, R. Arakawa, R. Matsumoto, and Y. Fujimura participated in the data analysis. S. Nozaki wrote the first draft of the manuscript. S. Nozaki, M. Kato, H. Takano, H. Takahashi, H. Ito, H. Kashima and T. Suhara had discussions and corrected the manuscript. All authors contributed to and have approved the final manuscript.

Conflict of interest

All the authors have no conflict of interest.

Acknowledgement

We thank Mr. Katsuyuki Tanimoto, Mr. Takahiro Shiraishi, and Ms. Yoshiko Fukushima for their assistance in performing the PET experiments at the National Institute of Radiological Sciences.

References

American Psychiatric Association, 1994. Diagnostic and Statistical Manual of Mental Disorders DSM-IV. American Psychiatric Association, Washington, DC, USA.

Andreasen, N.C., O'Leary, D.S., Flaum, M., Nopoulos, P., Watkins, G.L., Boles Ponto, L.L., Hichwa, R.D., 1997. Hypofrontality in schizophrenia: distributed dysfunctional circuits in neuroleptic-naive patients. Lancet 349, 1730–1734.

Braff, D.L., Swerdlow, N.R., Geyer, M.A., 1999. Symptom correlates of prepulse inhibition deficits in male schizophrenic patients. Am. J. Psychiatry 156, 596–602.

Breier, A., Su, T.P., Saunders, R., Carson, R.E., Kolachana, B.S., de Bartolomeis, A., Weinberger, D.R., Weisenfeld, N., Malhotra, A.K., Eckelman, W.C., Pickar, D., 1997. Schizophrenia is associated with elevated amphetamine-induced synaptic dopamine concentrations: evidence from a novel positron emission tomography method. Proc. Natl. Acad. Sci. U. S. A. 94, 2569–2574.

Buchsbaum, M.S., Someya, T., Teng, C.Y., Abel, L., Chin, S., Najafi, A., Haier, R.J., Wu, J., Bunney Jr., W.E., 1996. PET and MRI of the thalamus in never-medicated patients with schizophrenia. Am. J. Psychiatry 153, 191–199.

Buchsbaum, M.S., Christian, B.T., Lehrer, D.S., Narayanan, T.K., Shi, B., Mantil, J., Kemether, E., Oakes, T.R., Mukherjee, J., 2006. D_2/ D_3 dopamine receptor binding with [^{18}F]fallypride in thalamus and cortex of patients with schizophrenia. Schizophr. Res. 85, 232–244.

Carlsson, A., Waters, N., Waters, S., Carlsson, M.L., 2000. Network interactions in schizophrenia — therapeutic implications. Brain Res. Brain Res. Rev. 31, 342–349.

Clark, C., Kopala, L., Li, D.K., Hurwitz, T., 2001. Regional cerebral glucose metabolism in never-medicated patients with schizophrenia. Can. J. Psychiatry 46, 340–345.

Clinton, S.M., Meador-Woodruff, J.H., 2004. Thalamic dysfunction in schizophrenia: neurochemical, neuropathological, and in vivo imaging abnormalities. Schizophr. Res. 69, 237–253.

Dao-Castellana, M.H., Paillere-Martinot, M.L., Hantraye, P., Attar-Levy, D., Remy, P., Crouzel, C., Artiges, E., Feline, A., Syrota, A., Martinot, J.L., 1997. Presynaptic dopaminergic function in the striatum of schizophrenic patients. Schizophr. Res. 23, 167–174.

Dhawan, V., Ishikawa, T., Patlak, C., Chaly, T., Robeson, W., Belakhlef, A., Margouleff, C., Mandel, F., Eidelberg, D., 1996. Combined FDOPA and 3OMFD PET studies in Parkinson's disease. J. Nucl. Med. 37, 209–216.

Elkashef, A.M., Doudet, D., Bryant, T., Cohen, R.M., Li, S.H., Wyatt, R.J., 2000. 6-(18)F-DOPA PET study in patients with schizophrenia. Positron emission tomography. Psychiatry Res. 100, 1–11.

Farde, L., Wiesel, F.A., Stone-Elander, S., Halldin, C., Nordström, A.L., Hall, H., Sedvall, G., 1990. D_2 dopamine receptors in neuroleptic-naive schizophrenic patients. A positron emission tomography study with [^{11}C] raclopride. Arch. Gen. Psychiatry 47, 213–219.

First, M.B., Spitzer, R.L., Gibbon, M., Williams, J.B.W., 1997. User's Guide for the Structured Clinical Interview for DSM-IV Axis I Disorders: SCID-1 Clinician Version. American Psychiatric Publishing, Inc., Arlington, USA.

Gefvert, O., Lindström, L.H., Waters, N., Waters, S., Carlsson, A., Tedroff, J., 2003. Different corticostriatal patterns of L-DOPA utilization in patients with untreated schizophrenia and patients treated with classical antipsychotics or clozapine. Scand. J. Psychol. 44, 289–292.

Gjedde, A., 1982. Calculation of cerebral glucose phosphorylation from brain uptake of glucose analogs in vivo: a re-examination. Brain Res. 257, 237–274.

Gründer, G., Vernaleken, I., Muller, M.J., Davids, E., Heydari, N., Buchholz, H.G., Bartenstein, P., Munk, O.L., Stoeter, P., Wong, D.F., Gjedde, A., Cumming, P., 2003. Subchronic haloperidol downregulates dopamine synthesis capacity in the brain of schizophrenic patients in vivo. Neuropsychopharmacology 28, 787–794.

Hazlett, E.A., Buchsbaum, M.S., Byne, W., Wei, T.C., Spiegel-Cohen, J., Geneve, C., Kinderlehrer, R., Haznedar, M.M., Shihabuddin, L., Siever, L.J., 1999. Three-dimensional analysis with MRI and PET of the size, shape, and function of the thalamus in the schizophrenia spectrum. Am. J. Psychiatry 156, 1190–1199.

Hazlett, E.A., Buchsbaum, M.S., Kemether, E., Bloom, R., Platholi, J., Brickman, A.M., Shihabuddin, L., Tang, C., Byne, W., 2004. Abnormal glucose metabolism in the mediodorsal nucleus of the thalamus in schizophrenia. Am. J. Psychiatry 161, 305–314.

Hietala, J., Syvalahti, E., Vuorio, K., Rakkolainen, V., Bergman, J., Haaparanta, M., Solin, O., Kuoppamaki, M., Kirvela, O., Ruotsalainen, U., Salokangas, R., 1995. Presynaptic dopamine function in striatum of neuroleptic-naive schizophrenic patients. Lancet 346, 1130–1131.

Hietala, J., Syvalahti, E., Vilkman, H., Vuorio, K., Rakkolainen, V., Bergman, J., Haaparanta, M., Solin, O., Kuoppamaki, M., Eronen, E., Ruotsalainen, U., Salokangas, R.K., 1999. Depressive symptoms and presynaptic dopamine function in neuroleptic-naive schizophrenia. Schizophr. Res. 35, 41–50.

Igarashi, Y., Hayashi, N., Yamashina, M., Otsuka, N., Kuroki, N., Anzai, N., Kazamatsuri, H., 1998. Interrater reliability of the Japanese version of the positive and negative syndrome scale and the appraisal of its training effect. Psychiatry Clin. Neurosci. 52, 467–470.

Ito, H., Ota, M., Ikoma, Y., Seki, C., Yasuno, F., Takano, A., Maeda, J., Nakao, R., Suzuki, K., Suhara, T., 2006. Quantitative analysis of dopamine synthesis in human brain using positron emission tomography with L-[beta-^{11}C] DOPA. Nucl. Med. Commun. 27, 723–731.

Kim, J.J., Mohamed, S., Andreasen, N.C., O'Leary, D.S., Watkins, G.L., Boles Ponto, L.L., Hichwa, R.D., 2000. Regional neural dysfunctions in chronic schizophrenia studied with positron emission tomography. Am. J. Psychiatry 157, 542–548.

Kircher, T.T., Liddle, P.F., Brammer, M.J., Williams, S.C., Murray, R.M., McGuire, P.K., 2002. Reversed lateralization of temporal activation during speech production in thought disordered patients with schizophrenia. Psychol. Med. 32, 439–449.

Kumakura, Y., Cumming, P., Vernaleken, I., Buchholz, H.G., Siessmeier, T., Heinz, A., Kienast, T., Bartenstein, P., Gründer, G., 2007. Elevated [^{18}F] fluorodopamine turnover in brain of patients with schizophrenia: an [^{18}F]fluorodopa/positron emission tomography study. J. Neurosci. 27, 8080–8087.

Laakso, A., Vilkman, H., Alakare, B., Haaparanta, M., Bergman, J., Solin, O., Peurasaari, J., Rakkolainen, V., Syvalahti, E., Hietala, J., 2000. Striatal dopamine transporter binding in neuroleptic-naive patients with schizophrenia studied with positron emission tomography. Am. J. Psychiatry 157, 269–271.

Laakso, A., Vilkman, H., Bergman, J., Haaparanta, M., Solin, O., Syvalahti, E., Salokangas, R.K., Hietala, J., 2002. Sex differences in striatal presynaptic dopamine synthesis capacity in healthy subjects. Biol. Psychiatry 52, 759–763.

Laruelle, M., Abi-Dargham, A., van Dyck, C.H., Gil, R., D'Souza, C.D., Erdos, J., McCance, E., Rosenblatt, W., Fingado, C., Zoghbi, S.S., Baldwin, R.M., Seibyl, J.P., Krystal, J.H., Charney, D.S., Innis, R.B., 1996. Single photon emission computerized tomography imaging of amphetamine-induced dopamine release in drug-free schizophrenic subjects. Proc. Natl. Acad. Sci. U. S. A. 93, 9235–9240.

Laruelle, M., Abi-Dargham, A., van Dyck, C., Gil, R., D'Souza, D.C., Krystal, J., Seibyl, J., Baldwin, R., Innis, R., 2000. Dopamine and serotonin transporters in patients with schizophrenia: an imaging study with [^{123}I]beta-CIT. Biol. Psychiatry 47, 371–379.

Lindström, L.H., Gefvert, O., Hagberg, G., Lundberg, T., Bergstrom, M., Hartvig, P., Langström, B., 1999. Increased dopamine synthesis rate in medial prefrontal cortex and striatum in schizophrenia indicated by L-(beta-^{11}C) DOPA and PET. Biol. Psychiatry 46, 681–688.

Mai, J., Assheuer, J., Paxinos, G., 1997. Atlas of the Human Brain. Academic Press, New York.

McGowan, S., Lawrence, A.D., Sales, T., Quested, D., Grasby, P., 2004. Presynaptic dopaminergic dysfunction in schizophrenia: a positron emission tomographic [^{18}F]fluorodopa study. Arch. Gen. Psychiatry 61, 134–142.

McGraw, K.O., Wong, S.P., 1996. Forming inferences about some intraclass correlation coefficients. Psychol. Methods 1, 30–46.

Melega, W.P., Luxen, A., Perlmutter, M.M., Nissenson, C.H., Phelps, M.E., Barrio, J.R., 1990. Comparative in vivo metabolism of 6-[^{18}F]fluoro-L-dopa and [^{3}H]L-dopa in rats. Biochem. Pharmacol. 39, 1853–1860.

Mitelman, S.A., Byne, W., Kemether, E.M., Hazlett, E.A., Buchsbaum, M.S., 2005. Metabolic disconnection between the mediodorsal nucleus of the thalamus and cortical Brodmann's areas of the left hemisphere in schizophrenia. Am. J. Psychiatry 162, 1733–1735.

Nordström, A.L., Farde, L., Eriksson, L., Halldin, C., 1995. No elevated D_2 dopamine receptors in neuroleptic-naive schizophrenic patients revealed by positron emission tomography and [^{11}C]N-methylspiperone. Psychiatry Res. 61, 67–83.

Oldfield, R.C., 1971. The assessment and analysis of handedness: the Edinburgh Inventory. Neuropsychologia 9, 97–113.

Ota, M., Yasuno, F., Ito, H., Seki, C., Nozaki, S., Asada, T., Suhara, T., 2006. Age-related decline of dopamine synthesis in the living human brain measured by positron emission tomography with L-[beta-^{11}C]DOPA. Life Sci. 79, 730–736.

Parent, A., 1990. Extrinsic connections of the basal ganglia. Trends Neurosci. 13, 254–258.

Patlak, C.S., Blasberg, R.G., 1985. Graphical evaluation of blood-to-brain transfer constants from multiple-time uptake data. Generalizations. J. Cereb. Blood Flow Metab. 5, 584–590.

Reith, J., Benkelfat, C., Sherwin, A., Yasuhara, Y., Kuwabara, H., Andermann, F., Bachneff, S., Cumming, P., Diksic, M., Dyve, S.E., Etienne, P., Evans, A.C., Lal, S., Shevell, M., Savard, G., Wong, D.F., Chouinard, G., Gjedde, A., 1994. Elevated dopa decarboxylase activity in living brain of patients with psychosis. Proc. Natl. Acad. Sci. U. S. A. 91, 11651–11654.

Resnick, S.M., Gur, R.E., Alavi, A., Gur, R.C., Reivich, M., 1988. Positron emission tomography and subcortical glucose metabolism in schizophrenia. Psychiatry Res. 24, 1–11.

Salem, J.E., Kring, A.M., 1998. The role of gender differences in the reduction of etiologic heterogeneity in schizophrenia. Clin. Psychol. Rev. 18, 795–819.

Salokangas, R.K., Vilkman, H., Ilonen, T., Taiminen, T., Bergman, J., Haaparanta, M., Solin, O., Alanen, A., Syvalahti, E., Hietala, J., 2000. High levels of dopamine activity in the basal ganglia of cigarette smokers. Am. J. Psychiatry 157, 632–634.

Schmitt, G.J., Meisenzahl, E.M., Frodl, T., La Fougere, C., Hahn, K., Moller, H.J., Dresel, S., 2005. The striatal dopamine transporter in first-episode, drug-naive schizophrenic patients: evaluation by the new SPECT-ligand[^{99m}Tc] TRODAT-1. J. Psychopharmacol. 19, 488–493.

Shergill, S.S., Brammer, M.J., Williams, S.C., Murray, R.M., McGuire, P.K., 2000. Mapping auditory hallucinations in schizophrenia using functional magnetic resonance imaging. Arch. Gen. Psychiatry 57, 1033–1038.

Suhara, T., Okubo, Y., Yasuno, F., Sudo, Y., Inoue, M., Ichimiya, T., Nakashima, Y., Nakayama, K., Tanada, S., Suzuki, K., Halldin, C., Farde, L., 2002. Decreased dopamine D_2 receptor binding in the anterior cingulate cortex in schizophrenia. Arch. Gen. Psychiatry 59, 25–30.

Takahashi, H., Higuchi, M., Suhara, T., 2006. The role of extrastriatal dopamine D_2 receptors in schizophrenia. Biol. Psychiatry 59, 919–928.

Talvik, M., Nordström, A.L., Olsson, H., Halldin, C., Farde, L., 2003. Decreased thalamic D_2/ D_3 receptor binding in drug-naive patients with schizophrenia: a PET study with [^{11}C]FLB 457. Int. J. Neuropsychopharmacol. 6, 361–370.

Talvik, M., Nordström, A.L., Okubo, Y., Olsson, H., Borg, J., Halldin, C., Farde, L., 2006. Dopamine D_2 receptor binding in drug-naive patients with schizophrenia examined with raclopride-C11 and positron emission tomography. Psychiatry Res. 148, 165–173.

Torstenson, R., Tedroff, J., Hartvig, P., Fasth, K.J., Langstrom, B., 1999. A comparison of ^{11}C-labeled L-DOPA and L-fluorodopa as positron emission tomography tracers for the presynaptic dopaminergic system. J. Cereb. Blood Flow Metab. 19, 1142–1149.

Tuppurainen, H., Kuikka, J., Viinamaki, H., Husso-Saastamoinen, M., Bergstrom, K., Tiihonen, J., 2003. Extrastriatal dopamine D_2/ D_3 receptor density and distribution in drug-naïve schizophrenic patients. Mol. Psychiatry 8, 453–455.

Wahl, L., Chirakal, R., Firnau, G., Garnett, E.S., Nahmias, C., 1994. The distribution and kinetics of [^{18}F]6-fluoro-3-O-methyl-L-dopa in the human brain. J. Cereb. Blood Flow Metab. 14, 664–670.

Wong, D.F., Wagner Jr., H.N., Tune, L.E., Dannals, R.F., Pearlson, G.D., Links, J.M., Tamminga, C.A., Broussolle, E.P., Ravert, H.T., Wilson, A.A., Toung, J.K., Malat, J., Williams, J.A., O'Tuama, L.A., Snyder, S.H., Kuhar, M.J., Gjedde, A., 1986. Positron emission tomography reveals elevated D_2 dopamine receptors in drug-naïve schizophrenics. Science 234, 1558–1563.

Woodruff, P.W., Wright, I.C., Bullmore, E.T., Brammer, M., Howard, R.J., Williams, S.C., Shapleske, J., Rossell, S., David, A.S., McGuire, P.K., Murray, R.M., 1997. Auditory hallucinations and the temporal cortical response to speech in schizophrenia: a functional magnetic resonance imaging study. Am. J. Psychiatry 154, 1676–1682.

Yang, Y.K., Yu, L., Yeh, T.L., Chiu, N.T., Chen, P.S., Lee, I.H., 2004. Associated alterations of striatal dopamine D_2/ D_3 receptor and transporter binding in drug-naive patients with schizophrenia: a dual-isotope SPECT study. Am. J. Psychiatry 161, 1496–1498.

Yasuno, F., Suhara, T., Okubo, Y., Sudo, Y., Inoue, M., Ichimiya, T., Takano, A., Nakayama, K., Halldin, C., Farde, L., 2004. Low dopamine D_2 receptor binding in subregions of the thalamus in schizophrenia. Am. J. Psychiatry 161, 1016–1022.

Young, K.A., Randall, P.K., Wilcox, R.E., 1995. Startle and sensorimotor correlates of ventral thalamic dopamine and GABA in rodents. Neuroreport 6, 2495–2499.

Behavioral/Systems/Cognitive

Effects of the Antipsychotic Risperidone on Dopamine Synthesis in Human Brain Measured by Positron Emission Tomography with L-[β-^{11}C]DOPA: A Stabilizing Effect for Dopaminergic Neurotransmission?

Hiroshi Ito, Harumasa Takano, Hidehiko Takahashi, Ryosuke Arakawa, Michie Miyoshi, Fumitoshi Kodaka, Masaki Okumura, Tatsui Otsuka, and Tetsuya Suhara

Clinical Neuroimaging Team, Molecular Neuroimaging Group, Molecular Imaging Center, National Institute of Radiological Sciences, Chiba 263-8555, Japan

Effects of antipsychotic drugs have widely been considered to be mediated by blockade of postsynaptic dopamine D_2 receptors. Effects of antipsychotics on presynaptic functions of dopaminergic neurotransmission might also be related to therapeutic effects of antipsychotics. To investigate the effects of antipsychotics on presynaptic functions of dopaminergic neurotransmission in relation with occupancy of dopamine D_2 receptors, changes in dopamine synthesis capacity by antipsychotics and occupancy of dopamine D_2 receptors were measured by positron emission tomography (PET) in healthy men. PET studies using [^{11}C]raclopride and L-[β-^{11}C]DOPA were performed under resting condition and oral administration of single dose of the antipsychotic drug risperidone on separate days. Although occupancy of dopamine D_2 receptors corresponding dose of risperidone was observed, the changes in dopamine synthesis capacity by the administration of risperidone were not significant, nor was the relation between the occupancy of dopamine D_2 receptors and these changes. A significant negative correlation was observed between the baseline dopamine synthesis capacity and the changes in dopamine synthesis capacity by risperidone, indicating that this antipsychotic can be assumed to stabilize the dopamine synthesis capacity. The therapeutic effects of risperidone in schizophrenia might be related to such stabilizing effects on dopaminergic neurotransmission responsivity.

Introduction

Effects of antipsychotic drugs have widely been considered to be mediated by blockade of postsynaptic dopamine D_2 receptors (Carlsson and Lindqvist, 1963; Creese et al., 1976; Seeman et al., 1976). This hypothesis has been supported by positron emission tomography (PET) studies to determine the occupancy of dopamine D_2 receptors in schizophrenia patients treated with first-generation antipsychotics, e.g., haloperidol (Farde et al., 1988; Baron et al., 1989) and second-generation antipsychotics, e.g., risperidone (Nyberg et al., 1993).

Effects of antipsychotics on presynaptic functions of dopaminergic neurotransmission might also be related to the therapeutic effects of antipsychotics. It has been reported that antipsychotic drugs, chlorpromazine and haloperidol, increased dopamine metabolites in mouse brain tissue (Carlsson and Lindqvist, 1963; O'Keeffe et al., 1970), and also that risperidone and clozapine increased dopamine release in rat brain (Hertel et al., 1996). Increases and decreases in the activity of aromatic L-amino acid decarboxylase (AADC) by antagonists and agonists of dopamine D_2 receptors were also observed in rat brain tissue, respectively (Zhu et al., 1992, 1993). The regional activity of AADC in brain indicating the dopamine synthesis capacity can be estimated using radiolabeled L-DOPA (Gjedde et al., 1991). Significant increases and decreases in dopamine synthesis capacities by antagonists and agonists of dopamine D_2 receptors were observed in animal studies using [^{3}H]DOPA, L-[β-^{11}C]DOPA, or 6-[^{18}F]fluoro-L-DOPA, respectively (Cumming et al., 1997; Torstenson et al., 1998; Danielsen et al., 2001). These findings indicate that pharmacological effects on dopaminergic autoreceptors might cause changes in the presynaptic dopamine synthesis capacity (Carlsson and Lindqvist, 1963).

Effects of antipsychotics on the dopamine synthesis capacity in brain have been investigated in human subjects. A significant increase in dopamine synthesis capacity after acute administration of antipsychotic drug haloperidol was observed using PET with 6-[^{18}F]fluoro-L-DOPA in healthy human subjects (Vernaleken et al., 2006). On the other hand, a significant decrease in dopamine synthesis capacity after chronic administration of haloperidol was observed using 6-[^{18}F]fluoro-L-DOPA in patients with schizophrenia (Gründer et al., 2003). A significant in-

Received Aug. 24, 2009; revised Sept. 26, 2009; accepted Sept. 30, 2009.

This study was supported in part by a Grant-in-Aid for Molecular Imaging Program from the Ministry of Education, Culture, Sports, Science and Technology (MEXT), Japanese government, and a Grant-in-Aid for Scientific Research (C) (No. 21591587) from the Japan Society for the Promotion of Science. We thank Katsuyuki Tanimoto, Takahiro Shiraishi, and Toshio Miyamoto for their assistance in performing the PET experiments at the National Institute of Radiological Sciences. We also thank Yoshiko Fukushima and Masako Fukushima of the National Institute of Radiological Sciences for their help as clinical research coordinators.

Correspondence should be addressed to Dr. Hiroshi Ito, Clinical Neuroimaging Team, Molecular Neuroimaging Group, Molecular Imaging Center, National Institute of Radiological Sciences, 4-9-1 Anagawa, Inage-ku, Chiba 263-8555, Japan. E-mail: hito@nirs.go.jp.

DOI:10.1523/JNEUROSCI.4172-09.2009

 0270-6474/09/2913730-05$15.00/0

crease in the plasma concentration of homovanillic acid after acute administration of antipsychotics, haloperidol or fluphenazine, was observed in patients with schizophrenia, indicating an increase in dopamine turnover (Davila et al., 1988; Pickar et al., 1988). During chronic administration, a significant decrease in the plasma concentration of homovanillic acid was also observed (Davila et al., 1988; Pickar et al., 1988). However, the effects of antipsychotics on the dopamine synthesis capacity have not been investigated in relation to the occupancy of dopamine D_2 receptors in human subjects.

Recently, we have validated quantitative analyses in L-[β-^{11}C]DOPA PET studies (Ito et al., 2006, 2007). In the present study, to elucidate changes in dopamine synthesis capacity by antipsychotics in relation to the occupancy of dopamine D_2 receptors, dopamine D_2 receptor bindings and dopamine synthesis capacities at resting condition and after oral administration of a single dose of the antipsychotic drug risperidone were measured in the same human subjects by PET with [^{11}C]raclopride and L-[β-^{11}C]DOPA, respectively.

Materials and Methods

Subjects. The study was approved by the Ethics and Radiation Safety Committees of the National Institute of Radiological Sciences, Chiba, Japan. Twelve healthy men (21–29 years of age, 24.3 ± 2.9 years [mean ± SD]) were recruited and written informed consent was obtained. The subjects were free of somatic, neurological or psychiatric disorders on the basis of their medical history and magnetic resonance (MR) imaging of the brain. They had no history of current or previous drug abuse according to interview.

PET procedures. All PET studies were performed with a Siemens ECAT Exact HR+ system, which provides 63 sections with an axial field of view of 15.5 cm (Brix et al., 1997). The intrinsic spatial resolution was 4.3 mm in-plane and 4.2 mm full-width at half maximum (FWHM) axially. With a Hanning filter (cutoff frequency: 0.4 cycle/pixel), the reconstructed in-plane resolution was 7.5 mm FWHM. Data were acquired in three-dimensional mode. Scatter was corrected (Watson et al., 1996). A 10 min transmission scan using a ^{68}Ge-^{68}Ga line source was performed for correction of attenuation. A head fixation device with thermoplastic attachments for individual fit minimized head movement during the PET measurements.

PET studies were performed under resting condition (baseline study) and oral administration of risperidone (drug challenge study) on separate days. The interval between the 2 studies was 7 d in 10 subjects, and 14 d in 2 subjects. In each study, both PET scans with [^{11}C]raclopride and L-[β-^{11}C]DOPA were performed sequentially. After intravenous rapid bolus injection of [^{11}C]raclopride, dynamic PET scanning was performed for 60 min. After 1 h from the end of the [^{11}C]raclopride PET measurement, dynamic PET scanning was performed for 89 min after intravenous rapid bolus injection of L-[b-^{11}C]DOPA. The frame sequence consisted of twelve 20 s frames, sixteen 1 min frames, and ten 4 min frames for [^{11}C]raclopride, and seven 1 min frames, five 2 min frames, four 3 min frames, and twelve 5 min frames for L-[β-^{11}C]DOPA. The radioactivity injected was 220–230 MBq and 342–395 MBq in the baseline studies, and 205–274 MBq and 344–388 MBq in the drug challenge studies for [^{11}C]raclopride and L-[β-^{11}C]DOPA, respectively. The specific radioactivity was 168–517 GBq/μmol and 26–88 GBq/μmol in the baseline studies, and 162–535 GBq/μmol and 39–90 GBq/μmol in the drug challenge studies for [^{11}C]raclopride and L-[β-^{11}C]DOPA, respectively. A venous blood sample was taken at the beginning of L-[β-^{11}C]DOPA PET scanning for measurement of natural neutral amino acid (NAA) concentration in plasma. NAA concentration was measured by HPLC (L-8500 amino acid analyzer system, Hitachi Corp.). The amino acids are phenylalanine, tryptophan, leucine, methionine, isoleucine, tyrosine, histidine, valine and threonine, which are transported via the same carrier at the blood–brain barrier as L-DOPA (Sugaya et al., 2001). A weighted sum of the NAAs, which was the L-DOPA corresponding concentration of the nine NAAs for the carrier system, was calculated according to our previous work (Ito et al., 2006).

Table 1. Dose of risperidone and ranges of occupancy of dopamine D_2 receptors

	Occupancy (%)	
Dose of risperidone (mg)	Putamen	Caudate
0.5	39–46%	33–44%
1.0	48–52%	48–60%
1.5	61–69%	63–71%
2.0	71–75%	75–79%

In the drug challenge studies, risperidone at 0.5–2.0 mg was orally administrated 2 h before the start of PET scanning with [^{11}C]raclopride. The dose of risperidone was 0.5 mg in 3 subjects, 1.0 mg in 3 subjects, 1.5 mg in 3 subjects, and 2.0 mg in 3 subjects. To estimate the plasma concentration of risperidone and its active metabolite (9-hydroxy-risperidone), venous blood sampling was performed at the start and end of each PET scan. The plasma concentrations of risperidone and 9-hydroxy-risperidone were determined by validated liquid chromatography coupled to tandem mass spectrometry (LC-MS/MS) method. Since risperidone and 9-hydroxy-risperidone have similar binding profiles to neuroreceptors (Leysen et al., 1994), the sum of their plasma concentrations was used as the plasma concentration of the antipsychotic drug in the present study.

All MR imaging studies were performed with a 1.5-tesla MR scanner (Philips Medical Systems, Best, The Netherlands). Three-dimensional volumetric acquisition of a T1-weighted gradient echo sequence produced a gapless series of thin transverse sections (echo time, 9.2 ms; repetition time, 21 ms; flip angle: 30°; field of view: 256 mm; acquisition matrix: 256 × 256; slice thickness: 1 mm).

Regions of interest. All MR images were coregistered to the PET images with the statistical parametric mapping (SPM2) system (Friston et al., 1990). Regions of interest (ROIs) were drawn on coregistered MR images and transferred to the PET images. ROIs were defined for the cerebellar cortex, putamen, caudate head, and occipital cortex. Each ROI was drawn in three adjacent sections and data were pooled to obtain the average radioactivity concentration for the whole volume of interest. To obtain regional time-activity curves, regional radioactivity was calculated for each frame, corrected for decay, and plotted versus time. In-house software was used to draw ROIs.

Calculation of occupancy of dopamine D_2 receptors. For both PET studies with [^{11}C]raclopride, the binding potential (BP_{ND}) was calculated by the reference tissue model method (Lammertsma et al., 1996; Lammertsma and Hume, 1996). With this method, the time-activity curve in the brain region is described by that in the reference region with no specific binding, assuming that both regions have the same level of non-displaceable radioligand binding:

$$C_i(t) = R_1 \cdot C_r(t) + \{k_2 - R_1 \cdot k_2/(1 + BP_{ND})\} \cdot C_r(t) \otimes \exp\{-k_2 \cdot t/(1 + BP_{ND})\},$$

where C_i is the radioactivity concentration in a brain region; C_r is the radioactivity concentration in the reference region; R_1 is the ratio of K_1/K_1' (K_1, influx rate constant for the brain region; K_1', influx rate constant for the reference region), k_2 is the efflux rate constant for the brain region, and $\otimes$ denotes the convolution integral. In this analysis, three parameters (BP_{ND}, R_1, and k_2) were estimated by nonlinear least-squares curve fitting. The cerebellum was used as a reference region. The occupancy of dopamine D_2 receptors by risperidone was calculated as follows:

$$\text{Occupancy (\%)} = 100 \cdot BP_{ND(baseline)} - BP_{ND(drug)})/BP_{ND(baseline)},$$

where $BP_{ND(baseline)}$ is the BP_{ND} value in the baseline study, and $BP_{ND(drug)}$ is the BP_{ND} value in the drug challenge study.

Calculation of dopamine synthesis capacity. The uptake rate constant for L-[β-^{11}C]DOPA indicating the dopamine synthesis capacity was estimated by graphical analysis (Patlak and Blasberg, 1985; Gjedde, 1988; Hartvig et al.,

1991), which allows for the calculation of the uptake rate constant k_i using time-activity data in a reference brain region with no irreversible binding. The k_i values can be estimated by using simple linear least-squares fitting as follows:

$$\frac{C_i(t)}{C_i'(t)} = k_i \cdot \frac{\int_0^t C_i'(\tau)d\tau}{C_i'(t)} + F \qquad t < t^*,$$

where C_i and C_i' are the total radioactivity concentrations in a brain region with and without irreversible binding, respectively, and t^* is the equilibrium time of the compartment for unchanged radiotracer in brain tissue. Plotting $C_i(t)/C_i'(t)$ versus $\int_0^t C_i'(\tau)d\tau/C_i'(t)$, after time t^* yields a straight line with the slope k_i and intercept F. In the present study, the occipital cortex was used as a reference region with no irreversible binding, because this region is known to have the lowest dopamine concentration (Brown et al., 1979) and lowest aromatic L-amino acid decarboxylase activity (Lloyd and Hornykiewicz, 1972). The range of equilibrium time t^* of 29–89 min was used (Ito et al., 2006, 2007). The percentage change in k_i by oral administration of risperidone was calculated as follows:

$$\% \text{ change} = 100 \cdot (k_{i(drug)} - k_{i(baseline)})/k_{i(baseline)},$$

where $k_{i(baseline)}$ is the k_i value in the baseline study, and $k_{i(drug)}$ is the k_i value in the drug challenge study.

Results

The ranges of occupancy of dopamine D_2 receptors in the striatum for each dose of risperidone measured by PET with [^{11}C]raclopride are given in Table 1. The occupancies of dopamine D_2 receptors ranged from 39% to 75% in the putamen and from 33% to 79% in the caudate. The sums of the plasma concentrations of risperidone and 9-hydroxy-risperidone during [^{11}C]raclopride and L-[β-^{11}C]DOPA PET studies, averaged between the start and end of each scanning, ranged from 3.8 to 23.1 ng/ml (12.2 ± 6.6 ng/ml, mean ± SD) and from 2.6 to 19.5 ng/ml (10.5 ± 5.8 ng/ml), respectively.

The uptake rate constant k_i of L-[β-^{11}C]DOPA in the striatum indicating the dopamine synthesis capacity for baseline and drug challenge study results are shown in Figure 1. The k_i values were 0.0136 ± 0.0017 min^{-1} and 0.0142 ± 0.0010 min^{-1} (mean ± SD) in the putamen and 0.0121 ± 0.0018 min^{-1} and 0.0125 ± 0.0015 min^{-1} in the caudate for baseline and drug challenge studies, respectively. No significant differences in k_i were observed between the two studies. Weighted sums of the natural neutral amino acids (NAAs) in plasma were 1251 ± 198 nmol/ml for the baseline studies and 1207 ± 199 nmol/ml (mean ± SD) for the drug challenge studies. No significant differences in values were observed between the two studies.

The relations between the occupancy of dopamine D_2 receptors and the percentage change in k_i by drug challenge are

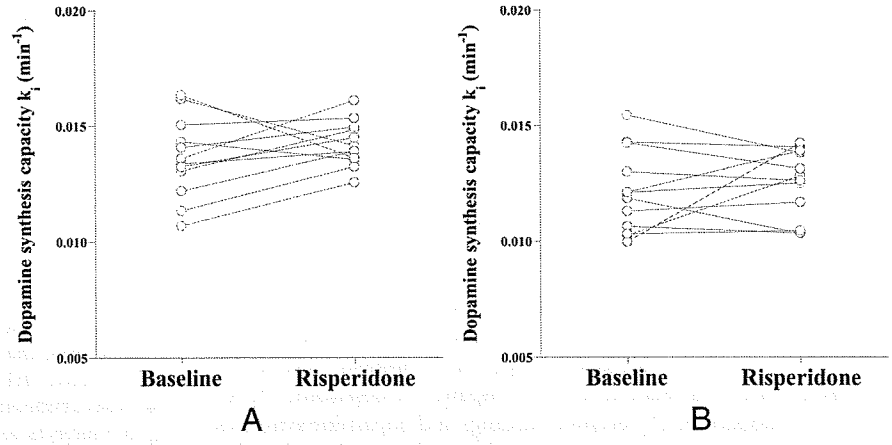

Figure 1. The uptake rate constant k_i indicating the dopamine synthesis capacity for the baseline study and drug challenge study with risperidone in the putamen (*A*) and caudate (*B*).

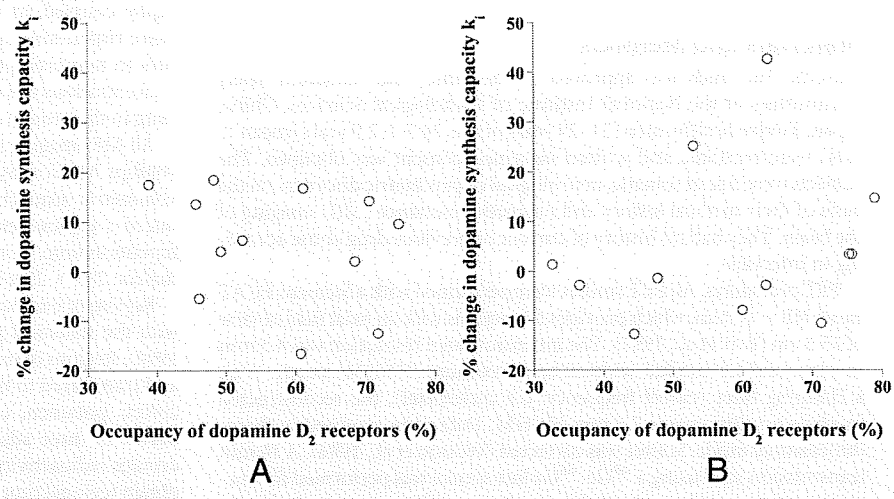

Figure 2. The relations between the occupancy of dopamine D_2 receptors and the percentage change in k_i by drug challenge with risperidone in the putamen (*A*) and caudate (*B*).

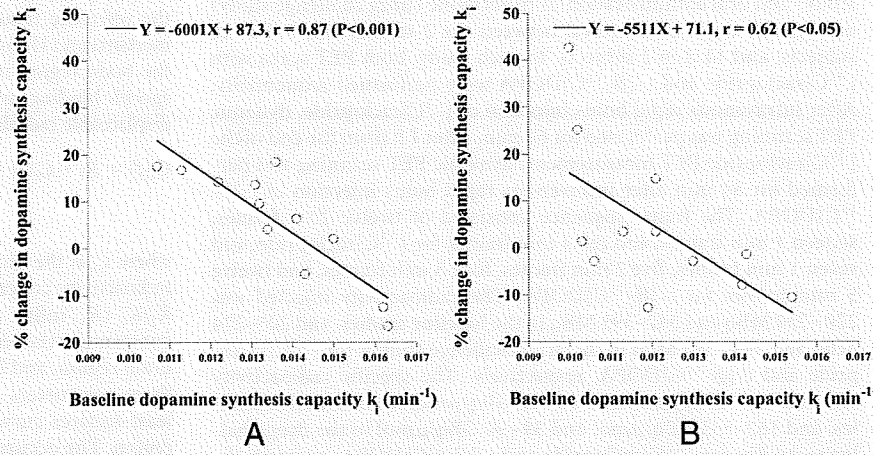

Figure 3. The relations between k_i in the baseline study and the percentage changes in k_i by drug challenge with risperidone in the putamen (*A*) and caudate (*B*).

shown in Figure 2. No significant correlations were observed. The relations between k_i in the baseline study and percentage change in k_i by the drug challenge are shown in Figure 3. Significant negative correlations were observed (putamen: $p < 0.001$, caudate: $p < 0.05$).

Discussion

Effects of antipsychotics on presynaptic dopamine synthesis might be caused by pharmacological activity on dopaminergic autoreceptors (Carlsson and Lindqvist, 1963). Although occupancy of dopamine D_2 receptors corresponding to the dose of risperidone was observed, no significant changes in the dopamine synthesis capacity k_i by administration of risperidone were observed in the present study. Furthermore, there were no significant correlations between the occupancy of dopamine D_2 receptors and changes in dopamine synthesis capacity k_i by risperidone. No significant changes in the dopamine synthesis capacity after acute administration of risperidone in healthy human subjects were also reported using 6-[^{18}F]-L-*m*-tyrosine (Mamo et al., 2004). On the other hand, a significant increase in the dopamine synthesis capacity measured using 6-[^{18}F]fluoro-L-DOPA and a significant increase in the plasma concentration of homovanillic acid have been observed after acute administration of antipsychotics, haloperidol or fluphenazine, in healthy human subjects (Vernaleken et al., 2006) and patients with schizophrenia (Davila et al., 1988; Pickar et al., 1988), respectively. The discrepancy between the present and previous results might have resulted from the use of different antipsychotics. However, in rat brain, it has been reported that risperidone and clozapine also increased dopamine release (Hertel et al., 1996). Another reason for this discrepancy might due to differences in the radiotracers used. However, in animal studies with [^{3}H]DOPA, L-[β-^{11}C]DOPA, or 6-[^{18}F]fluoro-L-DOPA, significant increases and decreases in dopamine synthesis capacities by antagonists and agonists of dopamine D_2 receptors, respectively, have been observed (Cumming et al., 1997; Torstenson et al., 1998; Danielsen et al., 2001).

In the present study, significant negative correlations were observed between the baseline dopamine synthesis capacity k_i and the percentage changes in the dopamine synthesis capacity by risperidone. This indicates that the increase and decrease in dopamine synthesis capacity by administration of risperidone are observed in subjects with low and high baseline dopamine synthesis capacity, respectively, and the degrees of increase and decrease in dopamine synthesis capacity are greater as the baseline dopamine synthesis capacities are smaller and larger, respectively. Negative correlations between baseline cerebral 6-[^{18}F]fluoro-L-DOPA utilization and change in 6-[^{18}F]fluoro-L-DOPA storage capacity by haloperidol challenge have also been observed in healthy human subjects (Vernaleken et al., 2008), corresponding to our present results. In addition, the coefficients of variation of dopamine synthesis capacity k_i were smaller in studies with the administration of risperidone than in baseline studies. Thus, the antipsychotic drug risperidone can be assumed to stabilize the dopamine synthesis capacity. The concept of phasic and tonic dopamine release with relation to the modulation of dopaminergic neurotransmission has been proposed, and abnormal responsivity in both phasic and tonic dopamine release in schizophrenia has been considered (Grace, 1991). The therapeutic effects of risperidone might be related to stabilizing effects on such dopaminergic responsivity. In addition, it has been reported that an antipsychotic drug, clozapine, normalized dopamine turnover in the primate phencyclidine model, indicating that the effects of clozapine in schizophrenia might be related to the restoration of dopamine tone (Elsworth et al., 2008). In this study, only an acute intervention was performed on healthy subjects, and therefore, the chronic effects of antipsychotics on patients with schizophrenia should be investigated in future.

It has been reported that the working memory and learning functions were correlated with the baseline dopamine synthesis capacity (Cools et al., 2008, 2009). Further studies to investigate the effects of antipsychotics on such higher brain functions in relation with changes in dopamine synthesis capacity should be considered (Vernaleken et al., 2008).

Serotonin 5-HT_{2A} receptor antagonists have been reported to modulate endogenous dopamine release (Pehek et al., 2001), and to reduce extrapyramidal side effects (Balsara et al., 1979; Korsgaard et al., 1985; Hicks, 1990). Risperidone is an antagonist for dopamine D_2 receptors and serotonin 5-HT_{2A} receptors with high affinity (Leysen et al., 1994), and it has been reported to modulate endogenous dopamine release. These findings indicate that changes in the dopamine synthesis capacity by administration of risperidone might be due to not only pharmacological effects on dopaminergic autoreceptors, but also on serotonin 5-HT_{2A} receptors. Thus, the stabilizing effects of risperidone on the dopamine synthesis level might also be related to its antagonism toward serotonin 5-HT_{2A} receptors. To elucidate this, further studies based on the same design using a selective antagonist for dopamine D_2 receptors, such as sulpiride, should be considered. In addition, a new antipsychotic drug aripiprazole that is a partial agonist to dopamine D_2 receptors has recently been used for treatment of schizophrenia (Mamo et al., 2007). Further studies to investigate the effects of aripiprazole on dopamine synthesis capacity should also be considered.

In conclusion, dopamine D_2 receptor bindings and dopamine synthesis capacities at resting condition and after oral administration of a single dose of the antipsychotic drug risperidone were measured in the same human subjects. Although occupancy of dopamine D_2 receptors corresponding to the dose of risperidone was observed, no significant changes in dopamine synthesis capacity by administration of risperidone were observed. It was also noted that there was no significant correlation between occupancy of dopamine D_2 receptors and changes in dopamine synthesis capacity by risperidone. On the other hand, a significant negative correlation was observed between the baseline dopamine synthesis capacity and the changes in dopamine synthesis capacity by risperidone. This indicates that the antipsychotic drug risperidone can be considered to stabilize the dopamine synthesis capacity. This suggests that the therapeutic effects of risperidone in schizophrenia might be related to the stabilizing effects on dopaminergic neurotransmission responsivity.

References

Balsara JJ, Jadhav JH, Chandorkar AG (1979) Effect of drugs influencing central serotonergic mechanisms on haloperidol-induced catalepsy. Psychopharmacology (Berl) 62:67–69.

Baron JC, Martinot JL, Cambon H, Boulenger JP, Poirier MF, Caillard V, Blin J, Huret JD, Loc'h C, Maziere B (1989) Striatal dopamine receptor occupancy during and following withdrawal from neuroleptic treatment: correlative evaluation by positron emission tomography and plasma prolactin levels. Psychopharmacology (Berl) 99:463–472.

Brix G, Zaers J, Adam LE, Bellemann ME, Ostertag H, Trojan H, Haberkorn U, Doll J, Oberdorfer F, Lorenz WJ (1997) Performance evaluation of a whole-body PET scanner using the NEMA protocol. J Nucl Med 38:1614–1623.

Brown RM, Crane AM, Goldman PS (1979) Regional distribution of monoamines in the cerebral cortex and subcortical structures of the rhesus monkey: concentrations and in vivo synthesis rates. Brain Res 168:133–150.

Carlsson A, Lindqvist M (1963) Effect of chlorpromazine or haloperidol on formation of 3-methoxytyramine and normetanephrine in mouse brain. Acta Pharmacol Toxicol (Copenh) 20:140–144.

Cools R, Gibbs SE, Miyakawa A, Jagust W, D'Esposito M (2008) Working memory capacity predicts dopamine synthesis capacity in the human striatum. J Neurosci 28:1208–1212.

Cools R, Frank MJ, Gibbs SE, Miyakawa A, Jagust W, D'Esposito M (2009) Striatal dopamine predicts outcome-specific reversal learning and its sensitivity to dopaminergic drug administration. J Neurosci 29:1538–1543.

Creese I, Burt DR, Snyder SH (1976) Dopamine receptor binding predicts clinical and pharmacological potencies of antischizophrenic drugs. Science 192:481–483.

Cumming P, Ase A, Laliberté C, Kuwabara H, Gjedde A (1997) In vivo regulation of DOPA decarboxylase by dopamine receptors in rat brain. J Cereb Blood Flow Metab 17:1254–1260.

Danielsen EH, Smith D, Hermansen F, Gjedde A, Cumming P (2001) Acute neuroleptic stimulates DOPA decarboxylase in porcine brain in vivo. Synapse 41:172–175.

Davila R, Manero E, Zumarraga M, Andia I, Schweitzer JW, Friedhoff AJ (1988) Plasma homovanillic acid as a predictor of response to neuroleptics. Arch Gen Psychiatry 45:564–567.

Elsworth JD, Jentsch JD, Morrow BA, Redmond DE Jr, Roth RH (2008) Clozapine normalizes prefrontal cortex dopamine transmission in monkeys subchronically exposed to phencyclidine. Neuropsychopharmacology 33:491–496.

Farde L, Wiesel FA, Halldin C, Sedvall G (1988) Central D_2-dopamine receptor occupancy in schizophrenic patients treated with antipsychotic drugs. Arch Gen Psychiatry 45:71–76.

Friston KJ, Frith CD, Liddle PF, Dolan RJ, Lammertsma AA, Frackowiak RS (1990) The relationship between global and local changes in PET scans. J Cereb Blood Flow Metab 10:458–466.

Gjedde A (1988) Exchange diffusion of large neutral amino acids between blood and brain. In: Peptide and amino acid transport mechanisms in the cerebral nervous system (Rakic L, Begley DJ, Davson H, Zlokovic BV, eds), pp 209–217. New York: Stockton.

Gjedde A, Reith J, Dyve S, Leger G, Guttman M, Diksic M, Evans A, Kuwabara H (1991) Dopa decarboxylase activity of the living human brain. Proc Natl Acad Sci U S A 88:2721–2725.

Grace AA (1991) Phasic versus tonic dopamine release and the modulation of dopamine system responsivity: a hypothesis for the etiology of schizophrenia. Neuroscience 41:1–24.

Gründer G, Vernaleken I, Müller MJ, Davids E, Heydari N, Buchholz HG, Bartenstein P, Munk OL, Stoeter P, Wong DF, Gjedde A, Cumming P (2003) Subchronic haloperidol downregulates dopamine synthesis capacity in the brain of schizophrenic patients in vivo. Neuropsychopharmacology 28:787–794.

Hartvig P, Agren H, Reibring L, Tedroff J, Bjurling P, Kihlberg T, Långström B (1991) Brain kinetics of L-[β-^{11}C]dopa in humans studied by positron emission tomography. J Neural Transm Gen Sect 86:25–41.

Hertel P, Nomikos GG, Iurlo M, Svensson TH (1996) Risperidone: regional effects in vivo on release and metabolism of dopamine and serotonin in the rat brain. Psychopharmacology (Berl) 124:74–86.

Hicks PB (1990) The effect of serotonergic agents on haloperidol-induced catalepsy. Life Sci 47:1609–1615.

Ito H, Ota M, Ikoma Y, Seki C, Yasuno F, Takano A, Maeda J, Nakao R, Suzuki K, Suhara T (2006) Quantitative analysis of dopamine synthesis in human brain using positron emission tomography with L-[β-^{11}C]DOPA. Nucl Med Commun 27:723–731.

Ito H, Shidahara M, Takano H, Takahashi H, Nozaki S, Suhara T (2007) Mapping of central dopamine synthesis in man using positron emission tomography with L-[β-^{11}C]DOPA. Ann Nucl Med 21:355–360.

Korsgaard S, Gerlach J, Christensson E (1985) Behavioral aspects of serotonin-dopamine interaction in the monkey. Eur J Pharmacol 118: 245–252.

Lammertsma AA, Hume SP (1996) Simplified reference tissue model for PET receptor studies. Neuroimage 4:153–158.

Lammertsma AA, Bench CJ, Hume SP, Osman S, Gunn K, Brooks DJ, Frackowiak RS (1996) Comparison of methods for analysis of clinical [^{11}C]raclopride studies. J Cereb Blood Flow Metab 16:42–52.

Leysen JE, Janssen PM, Megens AA, Schotte A (1994) Risperidone: a novel antipsychotic with balanced serotonin-dopamine antagonism, receptor occupancy profile, and pharmacologic activity. J Clin Psychiatry 55 (Suppl):5–12.

Lloyd KG, Hornykiewicz O (1972) Occurrence and distribution of aromatic L-amino acid (L-DOPA) decarboxylase in the human brain. J Neurochem 19:1549–1559.

Mamo D, Remington G, Nobrega J, Hussey D, Chirakal R, Wilson AA, Baker G, Houle S, Kapur S (2004) Effect of acute antipsychotic administration on dopamine synthesis in rodents and human subjects using 6-[^{18}F]-L-*m*-tyrosine. Synapse 52:153–162.

Mamo D, Graff A, Mizrahi R, Shammi CM, Romeyer F, Kapur S (2007) Differential effects of aripiprazole on D_2, 5-HT_2, and 5-HT_{1A} receptor occupancy in patients with schizophrenia: a triple tracer PET study. Am J Psychiatry 164:1411–1417.

Nyberg S, Farde L, Eriksson L, Halldin C, Eriksson B (1993) 5-HT_2 and D_2 dopamine receptor occupancy in the living human brain. A PET study with risperidone. Psychopharmacology (Berl) 110:265–272.

O'Keeffe R, Sharman DF, Vogt M (1970) Effect of drugs used in psychoses on cerebral dopamine metabolism. Br J Pharmacol 38:287–304.

Patlak CS, Blasberg RG (1985) Graphical evaluation of blood-to-brain transfer constants from multiple-time uptake data. Generalizations. J Cereb Blood Flow Metab 5:584–590.

Pehek EA, McFarlane HG, Maguschak K, Price B, Pluto CP (2001) M100,907, a selective 5-HT_{2A} antagonist, attenuates dopamine release in the rat medial prefrontal cortex. Brain Res 888:51–59.

Pickar D, Breier A, Kelsoe J (1988) Plasma homovanillic acid as an index of central dopaminergic activity: studies in schizophrenic patients. Ann N Y Acad Sci 537:339–346.

Seeman P, Lee T, Chau-Wong M, Wong K (1976) Antipsychotic drug doses and neuroleptic/dopamine receptors. Nature 261:717–719.

Sugaya Y, Sasaki Y, Goshima Y, Kitahama K, Kusakabe T, Miyamae T, Kato T, Misu Y (2001) Autoradiographic studies using L-[^{14}C]DOPA and L-DOPA reveal regional Na^+-dependent uptake of the neurotransmitter candidate L-DOPA in the CNS. Neuroscience 104:1–14.

Torstenson R, Hartvig P, Långström B, Bastami S, Antoni G, Tedroff J (1998) Effect of apomorphine infusion on dopamine synthesis rate relates to dopaminergic tone. Neuropharmacology 37:989–995.

Vernaleken I, Kumakura Y, Cumming P, Buchholz HG, Siessmeier T, Stoeter P, Müller MJ, Bartenstein P, Gründer G (2006) Modulation of [^{18}F]fluorodopa (FDOPA) kinetics in the brain of healthy volunteers after acute haloperidol challenge. Neuroimage 30:1332–1339.

Vernaleken I, Kumakura Y, Buchholz HG, Siessmeier T, Hilgers RD, Bartenstein P, Cumming P, Gründer G (2008) Baseline [^{18}F]-FDOPA kinetics are predictive of haloperidol-induced changes in dopamine turnover and cognitive performance: a positron emission tomography study in healthy subjects. Neuroimage 40:1222–1231.

Watson CC, Newport D, Casey ME (1996) A single scatter simulation technique for scatter correction in 3D PET. In: Three-dimensional image reconstruction in radiology and nuclear medicine (Grangeat P, Amans JL, eds), pp 255–268. Dordrecht, The Netherlands: Kluwer Academic Publishers.

Zhu MY, Juorio AV, Paterson IA, Boulton AA (1992) Regulation of aromatic L-amino acid decarboxylase by dopamine receptors in the rat brain. J Neurochem 58:636–641.

Zhu MY, Juorio AV, Paterson IA, Boulton AA (1993) Regulation of striatal aromatic L-amino acid decarboxylase: effects of blockade or activation of dopamine receptors. Eur J Pharmacol 238:157–164.

Neuroscience Research xxx (2010) xxx–xxx

Contents lists available at ScienceDirect

Neuroscience Research

journal homepage: www.elsevier.com/locate/neures

Cerebral activation associated with speech sound discrimination during the diotic listening task: An fMRI study

Yumiko Ikeda [a], Noriaki Yahata [a,1], Hidehiko Takahashi [b], Michihiko Koeda [c], Kunihiko Asai [d], Yoshiro Okubo [c], Hidenori Suzuki [a,*]

[a] Department of Pharmacology, Nippon Medical School, 1-1-5, Sendagi, Bunkyo-ku, Tokyo 113-8602, Japan
[b] Department of Molecular Neuroimaging, Molecular Imaging Center, National Institute of Radiological Sciences, 4-9-1, Anagawa, Inage-ku, Chiba 263-8555, Japan
[c] Department of Neuropsychiatry, Nippon Medical School, 1-1-5, Sendagi, Bunkyo-ku, Tokyo 113-8602, Japan
[d] Asai Hospital, 38-1, Katoku, Togane, Chiba 283-0062, Japan

ARTICLE INFO

Article history:
Received 22 July 2009
Received in revised form 4 February 2010
Accepted 5 February 2010

Keywords:
Auditory attention
Diotic listening
Functional MRI
Left anterior superior temporal gyrus
Left inferior temporal gyrus
Right superior temporal gyrus

ABSTRACT

Comprehending conversation in a crowd requires appropriate orienting and sustainment of auditory attention to and discrimination of the target speaker. While a multitude of cognitive functions such as voice perception and language processing work in concert to subserve this ability, it is still unclear which cognitive components critically determine successful discrimination of speech sounds under constantly changing auditory conditions. To investigate this, we present a functional magnetic resonance imaging (fMRI) study of changes in cerebral activities associated with varying challenge levels of speech discrimination. Subjects participated in a diotic listening paradigm that presented them with two news stories read simultaneously but independently by a target speaker and a distracting speaker of incongruent or congruent sex. We found that the voice of distracter of congruent rather than incongruent sex made the listening more challenging, resulting in enhanced activities mainly in the left temporal and frontal gyri. Further, the activities at the left inferior, left anterior superior and right superior loci in the temporal gyrus were shown to be significantly correlated with accuracy of the discrimination performance. The present results suggest that the subregions of bilateral temporal gyri play a key role in the successful discrimination of speech under constantly changing auditory conditions as encountered in daily life.

1. Introduction

Selective listening is an auditory process that enables one to attend to a specific speech of interest among a mixture of parallel conversations. Accomplishment of this ability, commonly known as the cocktail party effect, requires not only appropriate orientation and sustainment of auditory attention but also a multitude of concomitant cognitive processes including sound discrimination, human voice recognition, language processing, and so forth. To reveal the underlying neural mechanisms, the so-called dichotic listening paradigm has long been used as an effective measure in combination with neuroimaging studies (Pugh et al., 1996; Beaman et al., 2007). In this paradigm, two different auditory stimuli are presented simultaneously, but with one of the stimuli delivered to one ear and the second to the other ear (Kimura, 1961; Bryden, 1988). The types of auditory stimuli ranged from simple tones (Jäncke et al., 2003; Petkov et al., 2004) to syllables (Lipschutz et al., 2002), to meaningful words (Grady et al., 1997; Jäncke et al., 2001), and to sentences (Hashimoto et al., 2000). Previous imaging studies based on this paradigm and using positron emission tomography (PET) and functional magnetic resonance imaging (fMRI) have revealed brain regions implicated in selective listening. Robust activity is observed in the bilateral temporal lobes, including the superior temporal gyrus (STG) (Tzourio et al., 1997; Alho et al., 1999; Hugdahl et al., 1999; Zatorre et al., 1999; Hashimoto et al., 2000; Jäncke et al., 2001; van den Noort et al., 2008) during dichotic listening tasks. These areas are well known to be involved in auditory perception (van den Noort et al., 2008). In addition, significant activation is found in the lateral frontal (Hashimoto et al., 2000; Lipschutz et al., 2002; Thomsen et al., 2004) and parietal cortices (Hashimoto et al., 2000; Lipschutz et al., 2002; van den Noort et al., 2008). Mid-ventrolateral (BA 45/47) and mid-dorsolateral areas (BA 9/46) in the lateral frontal cortex are involved in pruning out unwanted information by responding selectively to relevant information (Lipschutz et al., 2002). The parietal cortex, especially the temporoparietal junction extending toward the inferior parietal lobe (IPL), plays a major role in attentional orientation during dichotic listening (Lipschutz et al., 2002). Therefore,

* Corresponding author. Tel.: +81 3 3822 2131; fax: +81 3 5814 1684.
E-mail address: hsuzuki@nms.ac.jp (H. Suzuki).
[1] Present address: Department of Neuropsychiatry, Graduate School of Medicine, University of Tokyo, 7-3-1, Hongo, Bunkyo-ku, Tokyo 113-8655, Japan.

0168-0102/$ – see front matter © 2010 Elsevier Ireland Ltd and the Japan Neuroscience Society. All rights reserved.
doi:10.1016/j.neures.2010.02.006

Please cite this article in press as: Ikeda, Y., et al., Cerebral activation associated with speech sound discrimination during the diotic listening task: An fMRI study. Neurosci. Res. (2010), doi:10.1016/j.neures.2010.02.006

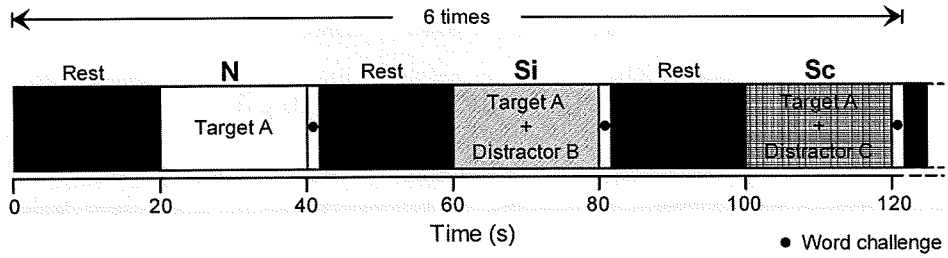

Fig. 1. The experimental block design of the session. Three conditions were sequentially presented to subjects: N, non-selective listening, a news story read out by a target speaker only; Si, selective listening, news stories read out by a target speaker and a distracting speaker of incongruent sex; Sc, selective listening, news stories read out by a target speaker and a distracting speaker of congruent sex. Each condition was presented for 20 s and interleaved with 20-s rest. After each condition, a word was displayed on a screen for 2 s (black circle) for the subjects to answer whether or not it was present in the target news of the preceding block by pressing a button. Each session was repeated six times.

the dichotic listening paradigm has a major advantage in specifying brain areas involved in the selective listening process, although speech discrimination under the constantly changing auditory conditions as encountered in daily life is far from such dichotic listening settings.

While the dichotic listening paradigm is one extreme abstraction of selective listening processes that we encounter in daily life, another experimental paradigm, the diotic listening paradigm, has also been used in previous studies, albeit less frequently, to investigate auditory attention under more natural listening settings. The task consists of binaural presentation of target stimuli superimposed by distracting stimuli (Scott et al., 2004; Shafiro and Gygi, 2007), so that the listening condition is more compatible with that in our daily life where the speech of interest and other conversations are typically mixed together and delivered to both ears. Previously, an fMRI study based on this paradigm reported that discrimination of human speech is associated with blood oxygenation level-dependent (BOLD) activation in Wernicke's area (BA22), Broca's area (BA44/45) and the frontal association cortex (BA6, 9/46, 32, 13/47), suggesting that the neural networks for executing semantic, syntactic, and prosodic processing are implicated in speech discrimination (Nakai et al., 2005). Given that constantly changing auditory environments are encountered in daily life, it is still unclear which brain regions critically work in response to change of challenge level in speech sound discrimination paradigms.

Here we present an fMRI study based on the diotic listening paradigm to evaluate brain activity involved in auditory selective attention. We found that hemodynamic activities in some temporal subregions showed significant correlations with performance accuracy of speech sound discrimination.

2. Materials and methods

2.1. Subjects

Twenty healthy volunteers, 10 males and 10 females, participated in the study (mean age ± SD, 24.9 ± 2.0 years). All subjects were right-handed according to the Edinburgh handedness inventory (mean laterality quotients ± SD, 89.7 ± 15.7) (Oldfield, 1971) and were native speakers of Japanese with normal hearing. None had a previous history of any neurological or psychiatric disorders. All subjects gave written informed consent prior to participation in the experiment. The present study was approved by the Ethics Committees of Nippon Medical School and Asai hospital.

2.2. Experimental design

The diotic listening task consisted of three conditions: (1) a reference condition wherein a single news story was read out by a target speaker (N condition), (2) a diotic listening condition wherein two distinct news stories were read out simultaneously but independently by the target and another speaker (distracter) of incongruent sex (Si condition), and (3) the same as Si condition except the sex of the distracter was congruent (Sc condition). Compared to the Si condition, the congruency of the sex of the speaker in the Sc condition was expected to make speech discrimination more challenging, since male and female reportedly have different phonation frequencies in reading possibly due to anatomical differences in vocal folds (Chen, 2007). The expected different levels of difficulty in speech sound discrimination were defined as 'challenge level' hereafter. The news stories were adopted from television programs and segmented into a 20-s long clip by a digital sound editor (Ulead MediaStudio Pro 6.0, Ulead Systems, Torrance, CA, USA). Each news segment contained 2.5 ± 2.3 sentences in each condition, which were read at a rate of 8.6 ± 0.6 characters/s.

A block design was used for the presentation of stimuli during the fMRI session. An active block of 20-s duration, corresponding to one of three listening conditions, was interleaved with resting periods of the same duration (Fig. 1). The order of conditions was fixed to N–Si–Sc, and this sequence was repeated six times in a single session (i.e., six news stories per condition). The target voice remained identical within a single sequence of conditions (N–Si–Sc), so the subjects could identify during the N condition which voice they should have attended to in the subsequent diotic listening conditions (Si and Sc). To avoid habituation to a particular voice, however, the target voices were altered across the sequences.

To quantify the degree of comprehension of stories read by the target voices, a word challenge was employed at each end of the block. A single word was visually presented for 2 s immediately after each block, and the subjects were required to judge if the word was present or absent in the preceding news segment.

The task presentation during the scan was controlled by SuperLab Pro 2.0.4 (Cedrus Corporation, San Pedro, CA, USA). Auditory stimuli were delivered binaurally through headphones (Resonance Technology Inc., Northridge, CA, USA). Visual stimuli were delivered to a translucent mirror attached to a head coil by a projector located outside the scanner room. During the scan, the subjects were instructed to use their index finger when answering the word challenge.

2.3. fMRI data acquisition

Functional imaging data were acquired with a 1.5 Tesla Signa system with a standard head coil (General Electric, Milwaukee, WI). Functional images of 180 volumes were acquired from each subject with T2*-weighted gradient-echo echo-planar imaging sequences sensitive to BOLD contrast. Each volume consisted of 40 transaxial contiguous sections with a section thickness of 3 mm to cover almost the whole brain (flip angle, 90°; TE, 50 ms; TR, 4 s; matrix, 64 × 64; field of view, 24 cm × 24 cm).

2.4. fMRI data analysis

Data analysis was performed with statistical parametric mapping software 2 (SPM2; Wellcome Department of Cognitive Neurology, University College London, UK) running with MATLAB (Mathworks, Natick, MA). All volumes were realigned to the first volume in each session to correct for head motion and were then spatially normalized to the standard space defined by the Montreal Neurological Institute template. After normalization, all scans had a resolution of 3 mm × 3 mm × 3 mm. Functional images were spatially smoothed with a 3D isotropic Gaussian kernel (full width at half maximum of 8 mm). Low frequency noise was removed by applying a high-pass filter (cutoff period, 80 s) to the fMRI time-series data of each voxel. For subject-level statistical analyses, significant hemodynamic changes in each condition (N, Si, Sc) were examined using the general linear model with boxcar functions convolved with a hemodynamic response function. Statistical parametric maps for each contrast (Si–N, Sc–N, Sc–Si) of the t-statistic were calculated on a voxel-by-voxel basis.

For group comparisons, random effect analyses were performed. The contrast images obtained from subject-level statistical analyses were entered into the random effects analyses. One-sample t-test was performed to determine group activation for each effect. A height threshold of $P < 0.001$ (uncorrected) and an extent threshold of 10 voxels were considered significant. For anatomical localization, peak voxels were converted from MNI to Talairach coordinates (Talairach and Tournoux, 1988).

Please cite this article in press as: Ikeda, Y., et al., Cerebral activation associated with speech sound discrimination during the diotic listening task: An fMRI study. Neurosci. Res. (2010), doi:10.1016/j.neures.2010.02.006

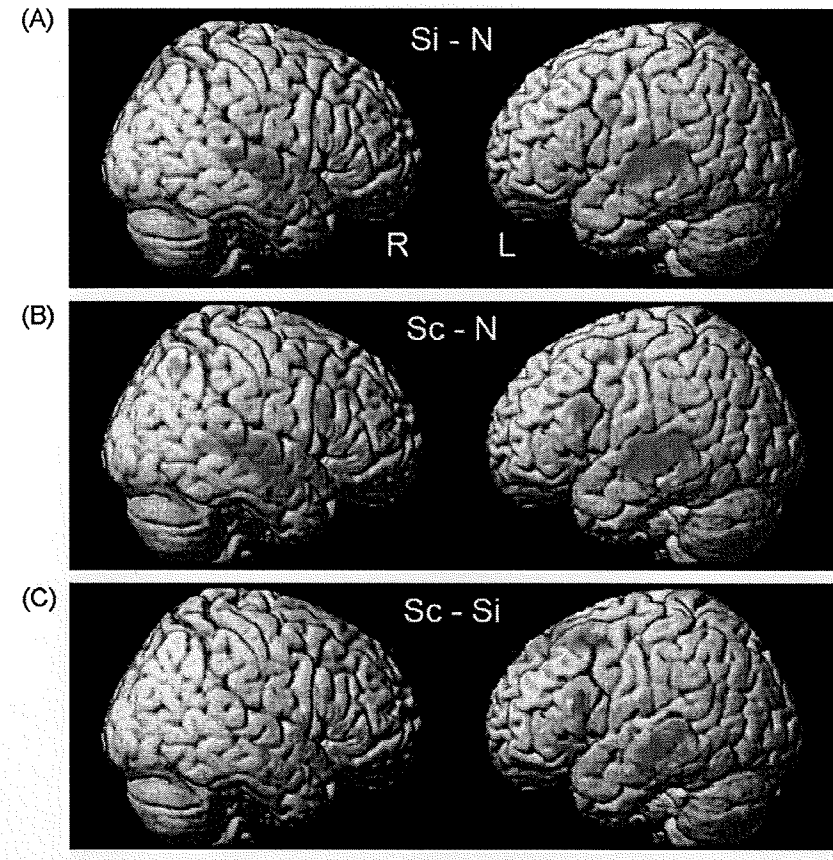

Fig. 2. Cortical rendering of activated areas in selective listening task. (A) Activation in the Si–N constrast. The bilateral temporal, frontal and parietal areas were activated. (B) Activation in the Sc–N contrast. The bilateral temporal, frontal areas, the left insula, cerebellum and the right parietal areas were activated. Compared with Si–N contrast, wider areas were activated in Sc–N contrast. (C) Activation in the Sc–Si contrast. The bilateral temporal, frontal areas and the left parietal areas were activated. All images are shown at the height threshold of $P = 0.001$, uncorrected, and the extent threshold of $k = 10$ voxels.

2.5. Performance analysis of word challenge

Performance score of the word challenge was obtained by counting the number of words that the subjects could answer correctly in the individual conditions with six repetitions. The accuracy rate was expressed as percent of the total number of correct words against all six sequences, and the values were shown as mean ± SD. The accuracy rate was compared among N, Si and Sc conditions using one-way ANOVA, followed by Tukey's multiple comparison test. $P < 0.05$ was considered statistically significant.

Simple regression analyses were performed to examine correlations between task-related BOLD signal changes of Sc–Si contrast and the performance score difference between Si and Sc conditions (Sc–Si). Pearson's correlation coefficient was then calculated with a significance threshold of $P < 0.05$.

3. Results

3.1. fMRI data

To assess the areas activated in selective listening attention under this designed experiment, the BOLD signal changes in both Si–N and Sc–N contrasts were examined. In Si–N contrast, as shown in Fig. 2A, the bilateral STG, middle temporal gyrus (MTG), middle frontal gyrus (MFG), superior parietal lobule (SPL), left precentral gyrus, right inferior frontal gyrus (IFG), precuneus and IPL were significantly activated (Table 1 and Fig. 2A). In Sc–N contrast, there was significant activation in the bilateral STG, MTG, IFG and MFG, the left insula and cerebellum, right medial frontal gyrus, precuneus, supramarginal gyrus (SMG) and inferior parietal gyrus (Table 1 and Fig. 2B). These results suggest that the brain regions activated in Sc condition are more widespread than those in Si condition.

Furthermore, the difference in BOLD signal between Sc and Si conditions was analyzed to reveal how the change of challenge level in speech sound discrimination affects brain hemodynamic activity. In Sc–Si contrast, significant activations were observed in the bilateral STG, MTG, IFG, MFG, medial frontal gyrus, SFG, left inferior temporal gyrus (ITG), SMG and IPL (Table 1 and Fig. 2C).

3.2. Accuracy rate

Next, we investigated whether the difference in challenge level in speech sound discrimination among three conditions reflects the difference in accuracy rate. The subjects judged the presence of the keywords in the preceding narration with 93.3 ± 8.4% (N condition), 92.5 ± 10.1% (Si), and 81.7 ± 17.1% (Sc) of accuracy rates, respectively (ANOVA for group comparison, $P = 0.0065$; Fig. 3). Thus, the subjects answered the target word less correctly in Sc condition than in N and Si conditions ($P < 0.05$), suggesting that they had more difficulty in discriminating the target voice when the distracter was of congruent sex in Sc condition.

3.3. Correlation between fMRI image and performance score

Further, we sought to determine the brain regions responsible for changes of challenge level in speech sound discrimination as measured by BOLD activation. The change in BOLD signal under Sc–Si contrast was positively correlated with the difference in performance score between Si and Sc conditions (Sc–Si) in the left ITG (BA 20, $R = 0.796$, $P < 0.001$), left anterior STG (BA 38, $R = 0.787$,

Please cite this article in press as: Ikeda, Y., et al., Cerebral activation associated with speech sound discrimination during the diotic listening task: An fMRI study. Neurosci. Res. (2010), doi:10.1016/j.neures.2010.02.006

Table 1
Regions activated in selective listening in Si–N, Sc–N and Sc–Si contrasts.

Contrast	Hemisphere	Region (Brodmann area)	Talairach			t-Value
			x	y	z	
Si–N	L	Superior temporal gyrus (22)	−59	−25	7	10.59
		Middle temporal gyrus (21)	−59	−6	−5	6.24
		Precentral gyrus (6/4)	−57	7	31	6.92
		Middle frontal gyrus (46)	−48	42	20	4.13
		Superior parietal lobule (7)	−12	−65	55	4.33
	R	Superior temporal gyrus (22/42)	61	−33	7	5.88
		Middle temporal gyrus (21)	67	−14	−4	5.73
		Middle frontal gyrus (10/9/46)	36	47	11	4.67
		Inferior frontal gyrus (44)	53	13	21	4.34
		Superior parietal lobule (7)	18	−69	50	6.65
		Precuneus (7)	16	−54	52	4.36
		Inferior parietal lobule (40)	57	−42	22	4.04
Sc–N	L	Superior temporal gyrus (22/42)	−51	−17	3	12.08
		Middle temporal gyrus (21)	−53	−12	−6	10.28
		Inferior frontal gyrus (45)	−57	20	19	8.01
		Middle frontal gyrus (6)	−46	4	50	6.24
		Insula	−30	19	−1	4.82
		Cerebellum	−14	−79	−21	5.39
	R	Middle temporal gyrus (21)	61	−6	−11	7.85
		Superior temporal gyrus (22/42)	63	−29	5	6.06
		Inferior frontal gyrus (45/44/47)	59	19	21	6.37
		Middle frontal gyrus (6/10/9/8/46)	48	8	46	5.09
		Medial frontal gyrus (8)	2	37	41	4.18
		Precuneus (7)	14	−62	40	4.85
		Supramarginal gyrus (40)	44	−43	37	4.67
		Inferior parietal lobule (39)	48	−58	43	4.45
Sc–Si	L	Middle temporal gyrus (21)	−55	−20	−7	6.66
		Superior temporal gyrus (22/38)	−46	−23	3	5.7
		Inferior temporal gyrus (20)	−46	−7	−25	4.47
		Inferior frontal gyrus (45/47)	−53	18	14	6.5
		Middle frontal gyrus (8/6)	−32	22	47	6.35
		Medial frontal gyrus (8)	−2	31	46	6.21
		Superior frontal gyrus (8/6)	−8	34	52	5.37
		Supramarginal gyrus (40)	−63	−47	28	5.56
		Inferior parietal lobule (39/40)	−50	−59	23	5.02
	R	Middle temporal gyrus (21)	53	1	−25	4.92
		Superior temporal gyrus (22)	46	−21	3	4.6
		Medial frontal gyrus (8/9)	2	39	40	5.08
		Superior frontal gyrus (8)	8	50	36	4.84
		Inferior frontal gyrus (45)	8	36	52	4.75
		Middle frontal gyrus (8/9/6/46)	61	22	21	4.44

$P<0.001$) and right STG (BA 22, $R=0.722$, $P<0.001$), respectively (Table 2 and Fig. 4). The two subregions in the left temporal gyrus (BA 20 and 38) were also included in activated areas under Sc–Si contrast by the overall analysis as shown in Table 1 (superior temporal gyrus and inferior temporal gyrus). At the individual level, 10 subjects showed no difference in the performance score between Sc and Si conditions, while they had increase in BOLD signal in the left ITG and left anterior STG under Sc–Si contrast (Fig. 4A and B). As for the right STG BOLD signal, seven subjects with lower performance score showed lower BOLD activity in this subregion under Sc condition than Si condition (Fig. 4C).

Table 2
Regions of activation correlated with performance score in Sc–Si contrast.

Hemisphere	Region (Brodmann area)	Talairach			t-Value
		x	y	z	
L	Inferior temporal gyrus (20)	−50	−32	−10	5.31
	Superior temporal gyrus (38)	−48	12	−28	4.46
R	Superior temporal gyrus (22)	63	−8	0	4.66

4. Discussion

4.1. Cortical network in auditory selective attention

By means of fMRI with a diotic experimental paradigm based rather on actual human conversation, cortical hemodynamic response was observed robustly in the bilateral STG and MTG and substantially in the bilateral MFG, right IFG and SPL in both Si and Sc conditions. Brain imaging (PET and fMRI) combined with dichotic listening task (O'Leary et al., 1996; Hugdahl et al., 1999, 2000; Hashimoto et al., 2000; Jäncke et al., 2001, 2003; Hund-Georgiadis et al., 2002) has already been extensively used to reveal the regions responsible for attentive listening. These studies have demonstrated widespread activities not only in the temporal cortex including bilateral STG and MTG, but also in the inferior parietal and prefrontal cortices (Jäncke and Shah, 2002; Lipschutz et al., 2002). In addition, an fMRI study (Nakai et al., 2005) using a diotic listening paradigm has also shown similar brain activation in the frontal association cortex as well as STG. Therefore, brain regions activated during the present diotic listening task are consistent with those previously reported, suggesting that the present task mimicking daily life conditions can efficiently activate the auditory attention networks commonly used during selective listening.

Please cite this article in press as: Ikeda, Y., et al., Cerebral activation associated with speech sound discrimination during the diotic listening task: An fMRI study. Neurosci. Res. (2010), doi:10.1016/j.neures.2010.02.006

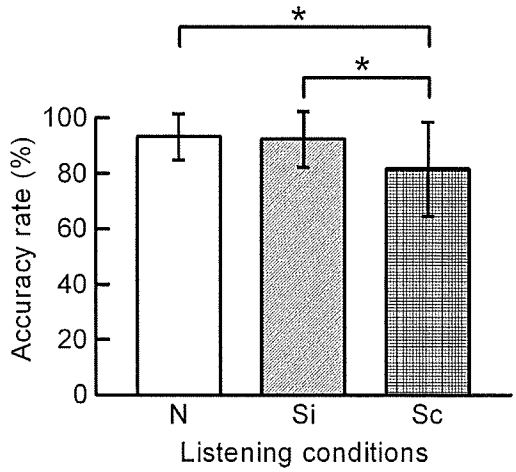

Fig. 3. Accuracy rate of word challenge. The ratio (%) of the number of target words correctly answered by the subjects in the individual conditions in the session was calculated and referred to as accuracy rate. The values were mean ± SD. The accuracy rates were significantly different among the three conditions ($F(2, 57) = 5.5$, $P = 0.0065$). Sc condition has significantly lower accuracy rate compared with N and Si conditions (*$P < 0.05$). N, non-selective listening; Si, selective listening with speakers of incongruent sex; Sc, selective listening with speakers of congruent sex. $n = 20$.

4.2. Diotic selective listening

To accomplish the diotic listening task in the present study, several distinct steps were required to process auditory information: discriminating the voice of the target speaker from that of the distracter, ignoring the distracter's voice, keeping attention focused on the story read by the target speaker, recognizing the words in the story, constructing sentences from the words, and comprehending and memorizing the sentences. In each process, distinct brain regions are thought to be involved. The right anterior part of the superior temporal sulcus and right IFG are reportedly involved in the prosodic component of speech sound processing (Plante et al., 2002; Zatorre et al., 2002) to discriminate the target voice by comparing it with others' prosodic features. The left frontal (BA 6, 8, 9, 44 and 46) and parietal lobes (BA7) have been thought to have a role in ignoring distracter stimuli (Bledowski et al., 2004). Broca's area (BA 44 and 45) is involved in syntactic processing (Stromswold et al., 1996; Caplan et al., 1999). It has been reported that the anterior areas of the left superior temporal gyrus and middle temporal gyrus are involved in speech comprehension (Scott et al., 2000; Davis and Johnsrude, 2003) and the left parietal cortex in working memory retrieval or short-time memory (Majerus et al., 2007; Öztekin et al., 2009). As shown by the results, the present task increased hemodynamic activation in the above-mentioned areas, consistent with the previous observations. Collectively, the present results suggest that the temporal, parietal and frontal regions are extensively involved in overall information processing during selective diotic listening.

However, there are several differences in the activated area between the previous dichotic listening studies and the present results. Activation of the primary auditory area such as BA 41 was not significant at the statistical threshold applied in the present study, while previous dichotic listening task studies found predominant activation in the primary auditory cortex contralateral to the ear of stimulation (Alho et al., 1999; Jäncke et al., 2001). Most of the auditory stimuli adopted in previous dichotic listening task studies were tone and syllables, whereas in the present task we used as stimuli two different contents of sentences read simultaneously but independently by a target and a distracting speaker. Under such condition, the subjects are required to execute neural processes pertaining to lexical access and semantic retrieval for completion of the task. Therefore, the cerebral activation might rather reflect post-sensory linguistic processing. In fact, functional neuroimaging studies using speech as stimuli showed activation of the left-lateralized networks, including the parietal, frontal and temporal cortex (Binder et al., 2009).

In addition, our results showed activation in the bilateral parietal cortices (BA 7) in Si–N contrast, the right parietal cortex (BA 39) in Sc–N contrast, and the left parietal cortex (BA 39 and 40) in Sc–Si contrast. While dichotic listening tasks have been reported to preferentially activate the right parietal cortex in association with spatial auditory processing (Alho and Vorobyev, 2007), left-dominant brain activation has been reported in angular gyrus (BA 39) and its adjacent areas (BA 40 and 7) in the semantic decision task using spoken languages (Binder et al., 1997, 2009). Accordingly, the parietal cortex activation shown in our task may be due to language processing rather than spatial processing.

4.3. Change of challenge level in speech sound discrimination and hemodynamic response in fMRI

As expected from the sex difference in voice properties, Sc condition was more difficult for the subjects to discriminate speech than Si condition when the mean accuracy rate in the performance was compared between Sc and Si conditions. Furthermore, the difference in performance between Si and Sc conditions was positively correlated with the change in BOLD signal under Sc–Si contrast in the left ITG, left anterior and right STG. At the individual level, half of the subjects showed increase in BOLD signal in the left ITG and left anterior STG without apparent difference in performance score between Sc and Si conditions. These results might be interpreted as the subjects making effort to attain good performance, resulting in BOLD increase in these regions. As described above, it has been reported that the left ITG and left anterior STG are involved in lexical–semantic processing (Binder et al., 2009). On the other hand, seven subjects with lower performance score under Sc condition than Si condition showed lower BOLD activity in the right STG. This implies that the activity of this subregion, which reportedly involves sentential prosody processing (Plante et al., 2002; Zatorre et al., 2002), may directly reflect the ability to discriminate performance. The involvement of these regions in successful discrimination may, therefore, indicate that the our present tasks require linguistic processing in addition to phonological one; since targeted words were presented in the news articles, the participants need to comprehend the target speech in the context of the news contents as well as to differentiate the target voice in the context of the phonetic feature. Collectively, these results suggest that these temporal subregions relating to language processing also play important roles in performing speech discrimination under constantly changing auditory conditions intermingled with different speakers' voices.

4.4. Selective auditory attention and psychiatric disorders

Patients with psychiatric disorders are known to often suffer from attention disturbance. For instance, deficit in attention has been thought to be a primary feature of neurocognitive profiles of patients with schizophrenia on the basis of neuropsychological studies (Heinrichs and Zakzanis, 1998; Fioravanti et al., 2005). Intriguingly, functional imaging studies of attention and working memory, however, have reported mixed findings in these patients. Attention task-related activation is attenuated in schizophrenia in DLPFC (Ojeda et al., 2002) and STG (Gallinat et al., 2002) as compared to in healthy subjects. In contrast, enhanced activa-

Please cite this article in press as: Ikeda, Y., et al., Cerebral activation associated with speech sound discrimination during the diotic listening task: An fMRI study. Neurosci. Res. (2010), doi:10.1016/j.neures.2010.02.006

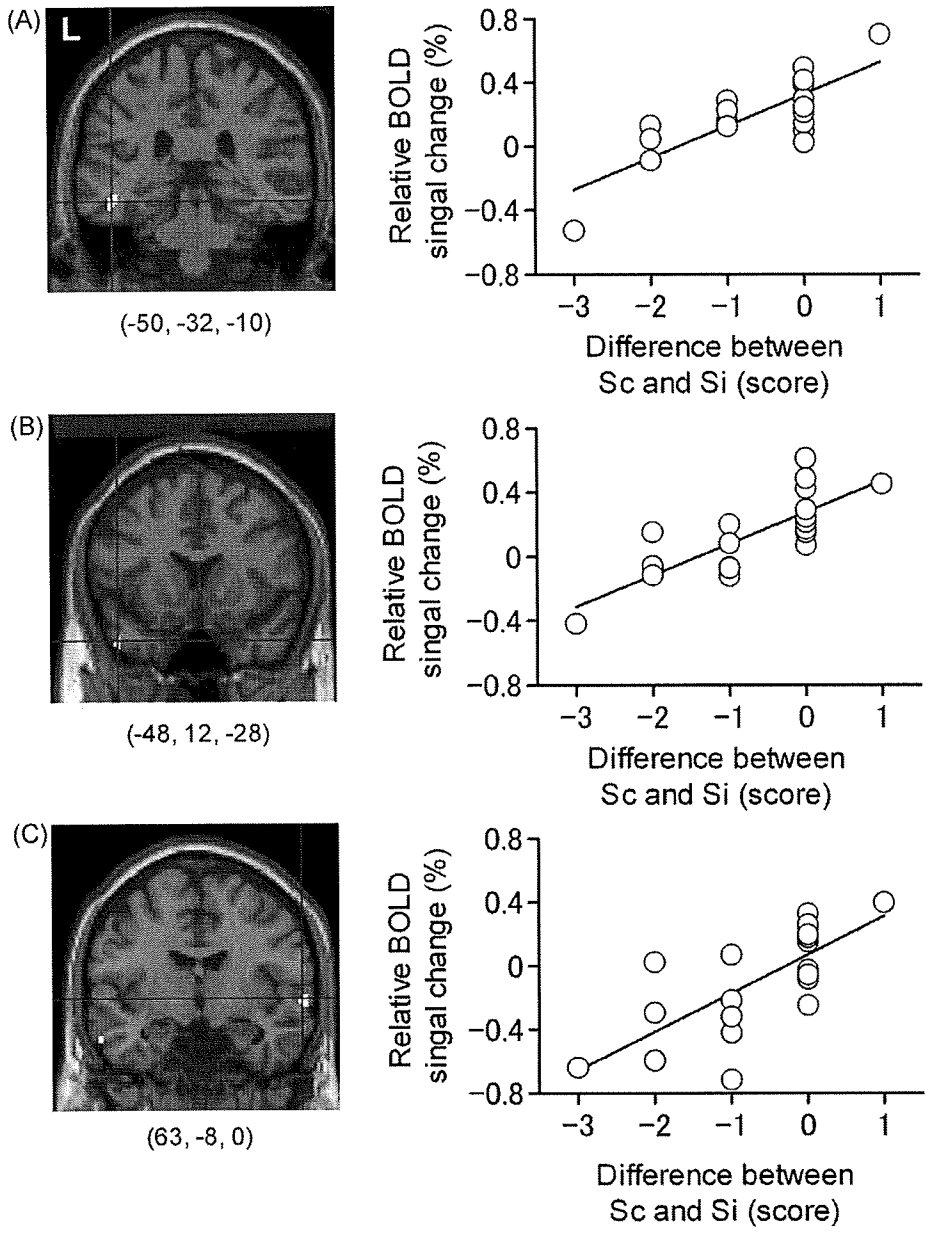

Fig. 4. Correlation between relative BOLD signal change and performance score difference in Sc–Si contrast. In the right panels, the vertical axes represent relative BOLD signal change in Sc–Si contrast, and the horizontal axes indicate the difference in performance score between Si and Sc conditions. Scatter plots illustrate significant positive correlations by simple regression analyses between neural activation of the left inferior temporal gyrus (A), left anterior superior temporal gyrus (B), or right superior temporal gyrus (C) and the performance score difference (Sc–Si). The left panels illustrate the brain regions with corresponding Talairach coordinates showing the correlations as described.

tion in DLPFC (Weiss et al., 2003) and STG (Weiss et al., 2007; Schirmer et al., 2009) has been observed in schizophrenia. Such discrepancy may be derived not only from the wide variety of patient profiles, but also task designs, which focus on different aspects of neurocognitive function of patients. A key feature of the paradigm used in the present study is that it could uniquely depict the brain activity during listening attention encountered in the daily conversational environment. In addition, this task can measure an activity change of the speech sound discrimination in temporal areas, which is reportedly reduced in volume in patients with schizophrenia (Collinson et al., 2009; Sun et al., 2009). Therefore, future studies using the present diotic task may be useful for investigating the cognitive aspect of auditory attention in patients with attention disturbance such as schizophrenia.

Acknowledgments

We thank the staffs of Asai hospital for their assistance in collecting the demographic data. Funding for this study was provided by a Grant-in-Aid for Science Research (C) from the Ministry of Education, Culture, Sports, Science, and Technology (MEXT), Japan, to H.S. (no. 1659028), a Grant-in-Aid for Encouragement of Young Scientists (B) from the Japan Society for the Promotion of Science (JSPS) to N.Y. (no. 18790852) and to Y.I. (no. 17790821).

References

Alho, K., Medvedev, S.V., Pakhomov, S.V., Roudas, M.S., Tervaniemi, M., Reinikainen, K., Zeffiro, T., Näätänen, R., 1999. Selective tuning of the left and right auditory cortices during spatially directed attention. Cogn. Brain Res. 7, 335–341.

Please cite this article in press as: Ikeda, Y., et al., Cerebral activation associated with speech sound discrimination during the diotic listening task: An fMRI study. Neurosci. Res. (2010), doi:10.1016/j.neures.2010.02.006

Alho, K., Vorobyev, V.A., 2007. Brain activity during selective listening to natural speech. Front. Biosci. 12, 3167–3176.
Beaman, C.P., Bridges, A.M., Scott, S.K., 2007. From dichotic listening to the irrelevant sound effect: a behavioural and neuroimaging analysis of the processing of unattended speech. Cortex 43, 124–134.
Binder, J.R., Frost, J.A., Hammeke, T.A., Cox, R.W., Rao, S.M., Prieto, T., 1997. Human brain language areas identified by functional magnetic resonance imaging. J. Neurosci. 17, 353–362.
Binder, J.R., Desai, R.H., Graves, W.W., Conant, L.L., 2009. Where is the semantic system? A critical review and meta-analysis of 120 functional neuroimaging studies. Cereb. Cortex 19, 2767–2796.
Bledowski, C., Prvulovic, D., Goebel, R., Zanella, F.E., Linden, D.E.J., 2004. Attentional systems in target and distractor processing: a combined ERP and fMRI study. Neuroimage 22, 530–540.
Bryden, M.P., 1988. Correlates of the dichotic right-ear effect. Cortex 24, 313–319.
Caplan, D., Alpert, N., Waters, G., 1999. PET studies of syntactic processing with auditory sentence presentation. Neuroimage 9, 343–351.
Chen, S.H., 2007. Sex differences in frequency and intensity in reading and voice range profiles for Taiwanese adult speakers. Folia Phoniatr. Logop. 59, 1–9.
Collinson, S.L., Mackay, C.E., Jiaqing, O., James, A.C.D., Crow, T.J., 2009. Dichotic listening impairments in early onset schizophrenia are associated with reduced left temporal lobe volume. Schizophr. Res. 112, 24–31.
Davis, M.H., Johnsrude, I.S., 2003. Hierarchical processing in spoken language comprehension. J. Neurosci. 23, 3423–3431.
Fioravanti, M., Carlone, O., Vitale, B., Cinti, M.E., Clare, L., 2005. A meta-analysis of cognitive deficits in adults with a diagnosis of schizophrenia. Neuropsychol. Rev. 15, 73–95.
Gallinat, J., Mulert, C., Bajbouj, M., Herrmann, W.M., Schunter, J., Senkowski, D., Moukhtieva, R., Kronfeldt, D., Winterer, G., 2002. Frontal and temporal dysfunction of auditory stimulus processing in schizophrenia. Neuroimage 17, 110–127.
Grady, C.L., Van Meter, J.W., Maisog, J.M., Pietrini, P., Krasuski, J., Rauschecker, J.P., 1997. Attention-related modulation of activity in primary and secondary auditory cortex. Neuroreport 8, 2511–2516.
Hashimoto, R., Homae, F., Nakajima, K., Miyashita, Y., Sakai, K.L., 2000. Functional differentiation in the human auditory and language areas revealed by a dichotic listening task. Neuroimage 12, 147–158.
Heinrichs, R.W., Zakzanis, K.K., 1998. Neurocognitive deficit in schizophrenia: a quantitative review of the evidence. Neuropsychology 12, 426–445.
Hugdahl, K., Brønnick, K., Kyllingsbæk, S., Law, I., Gade, A., Paulson, O.B., 1999. Brain activation during dichotic presentations of consonant–vowel and musical instrument stimuli: a ^{15}O-PET study. Neuropsychologia 37, 431–440.
Hugdahl, K., Law, I., Kyllingsbæk, S., Brønnick, K., Gade, A., Paulson, O.B., 2000. Effects of attention on dichotic listening: an ^{15}O-PET study. Hum. Brain Mapp. 10, 87–97.
Hund-Georgiadis, M., Lex, U., Friederici, A.D., von Cramon, D.Y., 2002. Non-invasive regime for language lateralization in right- and left-handers by means of functional MRI and dichotic listening. Exp. Brain Res. 145, 166–176.
Jäncke, L., Buchanan, T.W., Lutz, K., Shah, N.J., 2001. Focused and nonfocused attention in verbal and emotional dichotic listening: an FMRI study. Brain Lang. 78, 349–363.
Jäncke, L., Shah, N.J., 2002. Does dichotic listening probe temporal lobe functions? Neurology 58, 736–743.
Jäncke, L., Specht, K., Shah, J.N., Hugdahl, K., 2003. Focused attention in a simple dichotic listening task: an fMRI experiment. Cogn. Brain Res. 16, 257–266.
Kimura, D., 1961. Cerebral dominance and the perception of verbal stimuli. Can. J. Psychol. 15, 166–171.
Lipschutz, B., Kolinsky, R., Damhaut, P., Wikler, D., Goldman, S., 2002. Attention-dependent changes of activation and connectivity in dichotic listening. Neuroimage 17, 643–656.
Majerus, S., Bastin, C., Poncelet, M., Van der Linden, M., Salmon, E., Collette, F., Maquet, P., 2007. Short-term memory and the left intraparietal sulcus: focus of attention? Further evidence from a face short-term memory paradigm. Neuroimage 35, 353–367.
Nakai, T., Kato, C., Matsuo, K., 2005. An fMRI study to investigate auditory attention: a model of the cocktail party phenomenon. Magn. Reson. Med. Sci. 4, 75–82.
Ojeda, N., Ortuño, F., Arbizu, J., López, P., Martí-Climent, J.M., Peñuelas, I., Cervera-Enguix, S., 2002. Functional neuroanatomy of sustained attention in schizophrenia: contribution of parietal cortices. Hum. Brain Mapp. 17, 116–130.
O'Leary, D.S., Andreasen, N.C., Hurtig, R.R., Hichwa, R.D., Watkins, G.L., Ponto, L.L.B., Rogers, M., Kirchner, P.T., 1996. A positron emission tomography study of binaurally and dichotically presented stimuli: effects of level of language and directed attention. Brain Lang. 53, 20–39.
Oldfield, R.C., 1971. The assessment and analysis of handedness: the Edinburgh inventory. Neuropsychologia 9, 97–113.
Öztekin, I., McElree, B., Staresina, B.P., Davachi, L., 2009. Working memory retrieval: contributions of the left prefrontal cortex, the left posterior parietal cortex, and the hippocampus. J. Cogn. Neurosci. 21, 581–593.
Petkov, C.I., Kang, X., Alho, K., Bertrand, O., Yund, E.W., Woods, D.L., 2004. Attentional modulation of human auditory cortex. Nat. Neurosci. 7, 658–663.
Plante, E., Creusere, M., Sabin, C., 2002. Dissociating sentential prosody from sentence processing: activation interacts with task demands. Neuroimage 17, 401–410.
Pugh, K.R., Shaywitz, B.A., Shaywitz, S.E., Fulbright, R.K., Byrd, D., Skudlarski, P., Shankweiler, D.P., Katz, L., Constable, R.T., Fletcher, J., Lacadie, C., Marchione, K., Gore, J.C., 1996. Auditory selective attention: an fMRI investigation. Neuroimage 4, 159–173.
Schirmer, T.N., Dorflinger, J.M., Marlow-O'Connor, M., Pendergrass, J.C., Hartzell, A., All, S.D., Charles, D., 2009. FMRI indices of auditory attention in schizophrenia. Prog. Neuropsychopharmacol. Biol. Psychiatry 33, 25–32.
Scott, S.K., Blank, C.C., Rosen, S., Wise, R.J.S., 2000. Identification of a pathway for intelligible speech in the left temporal lobe. Brain 123, 2400–2406.
Scott, S.K., Rosen, S., Wichham, L., Wise, R.J.S., 2004. A positron emission tomography study of the neural basis of informational and energetic masking effects in speech perception. J. Acoust. Soc. Am. 115, 813–821.
Shafiro, V., Gygi, B., 2007. Perceiving the speech of multiple concurrent talkers in a combined divided and selective attention task. J. Acoust. Soc. Am. 122, EL229–EL235.
Stromswold, K., Caplan, D., Alpert, N., Rauch, S., 1996. Localization of syntactic comprehension by positron emission tomography. Brain Lang. 52, 452–473.
Sun, J., Maller, J.J., Guo, L., Fitzgerald, P.B., 2009. Superior temporal gyrus volume change in schizophrenia: a review on region of interest volumetric studies. Brain Res. Rev. 61, 14–32.
Talairach, J., Tournoux, P., 1988. Co-planar Stereotaxic Atlas of the Human Brain: 3-Dimensional Proportional System—An Approach to Cerebral Imaging. Thieme Medical Publishers, New York.
Thomsen, T., Rimol, L.M., Ersland, L., Hugdahl, K., 2004. Dichotic listening reveals functional specificity in prefrontal cortex: an fMRI study. Neuroimage 21, 211–218.
Tzourio, N., Massioui, F.E., Crivello, F., Joliot, M., Renault, B., Mazoyer, B., 1997. Functional anatomy of human auditory attention studied with PET. Neuroimage 5, 63–77.
van den Noort, M., Specht, K., Rimol, L.M., Ersland, L., Hugdahl, K., 2008. A new verbal reports fMRI dichotic listening paradigm for studies of hemispheric asymmetry. Neuroimage 40, 902–911.
Weiss, E.M., Golaszewski, S., Mottaghy, F.M., Hofer, A., Hausmann, A., Kemmler, G., Kremser, C., Brinkhoff, C., Felber, S.R., Fleischhacker, W.W., 2003. Brain activation patterns during a selective attention test—a functional MRI study in healthy volunteers and patients with schizophrenia. Psychiatry Res. Neuroimaging 123, 1–15.
Weiss, E.M., Siedentopf, C., Golaszewski, S., Mottaghy, F.M., Hofer, A., Kremser, C., Felber, S., Fleischhacker, W.W., 2007. Brain activation patterns during a selective attention test—a functional MRI study in healthy volunteers and unmedicated patients during an acute episode of schizophrenia. Psychiatry Res. Neuroimaging 154, 31–40.
Zatorre, R.J., Mondor, T.A., Evans, A.C., 1999. Auditory attention to space and frequency activates similar cerebral systems. Neuroimage 10, 544–554.
Zatorre, R.J., Belin, P., Penhune, V.B., 2002. Structure and function of auditory cortex: music and speech. Trends Cogn. Sci. 6, 37–46.

Please cite this article in press as: Ikeda, Y., et al., Cerebral activation associated with speech sound discrimination during the diotic listening task: An fMRI study. Neurosci. Res. (2010), doi:10.1016/j.neures.2010.02.006

Journal of Nuclear Medicine, published on April 16, 2009 as doi:10.2967/jnumed.108.058503

Quantitative PET Analysis of the Dopamine D_2 Receptor Agonist Radioligand ^{11}C-(*R*)-2-CH_3O-*N*-n-Propylnorapomorphine in the Human Brain

Tatsui Otsuka[1,2], Hiroshi Ito[1], Christer Halldin[3], Hidehiko Takahashi[1], Harumasa Takano[1], Ryosuke Arakawa[1], Masaki Okumura[1], Fumitoshi Kodaka[1], Michie Miyoshi[1], Mizuho Sekine[1], Chie Seki[1], Ryuji Nakao[4], Kazutoshi Suzuki[4], Sjoerd Finnema[3], Yoshio Hirayasu[2], Tetsuya Suhara[1], and Lars Farde[3]

[1]Molecular Neuroimaging Group, Molecular Imaging Center, National Institute of Radiological Sciences, Chiba, Japan; [2]Department of Psychiatry, Yokohama City University School of Medicine, Yokohama, Japan; [3]Psychiatry Section, Department of Clinical Neuroscience, Karolinska Institutet, Karolinska Hospital, Stockholm, Sweden; and [4]Molecular Probe Group, Molecular Imaging Center, National Institute of Radiological Sciences, Chiba, Japan

It has been demonstrated in vitro that the dopamine D_2 receptor has 2 interconvertible affinity states for endogenous dopamine, referred to as the high- and the low-affinity states. ^{11}C-(*R*)-2-CH_3O-*N*-n-propylnorapomorphine (^{11}C-MNPA) is a new agonist radioligand for in vivo imaging of the high-affinity state of dopamine D_2 receptors using PET. In the present study, the kinetics of ^{11}C-MNPA were examined for the first time, to our knowledge, in the human brain and analyzed using quantitative approaches with or without an arterial input function. **Methods:** A 90-min dynamic PET scan was obtained for 10 healthy men after an intravenous injection of ^{11}C-MNPA. The binding potential (BP_{ND}) was calculated using the indirect kinetic method, a kinetic compartment analysis with a metabolite-corrected arterial input function. BP_{ND} was also calculated by the simplified reference tissue model (SRTM) and transient equilibrium methods, both with the cerebellum as the reference brain region. The results of the quantitative methods were compared in a cross-validation approach. **Results:** The highest regional radioactivity was observed in the putamen. BP_{ND} values obtained by kinetic analysis were 0.82 ± 0.09, 0.59 ± 0.11, and 0.28 ± 0.06, respectively, in the putamen, caudate, and thalamus. BP_{ND} values obtained by the SRTM and transient equilibrium methods were in good agreement with those obtained by the indirect kinetic method (r = 0.98 and r = 0.93, respectively). For all quantification methods, the BP_{ND} values based on data acquired from 0 to 60 min were in good agreement with those based on data acquired from 0 to 90 min (r = 0.90–0.99). **Conclusion:** The regional distribution of ^{11}C-MNPA binding was in good agreement with previous PET studies of dopamine D_2 receptors in the human brain using antagonist radioligands. The results support routine use of the SRTM and transient equilibrium methods, that is, methods that do not require an arterial input function and need a scan time of only about 60 min. ^{11}C-MNPA should thus be useful for clinical research on the pathophysiology of neuropsychiatric disorders and estimation of dopamine D_2 receptor occupancy by dopaminergic drugs.

Key Words: ^{11}C-MNPA; agonist; dopamine D_2 receptor; positron emission tomography; human

J Nucl Med 2009; 50:703–710
DOI: 10.2967/jnumed.108.058503

The dopaminergic system in the brain plays a significant role in the physiologic regulation of motor functions, cognition, emotion, and personality (*1*). Alterations of dopaminergic neurotransmission have been implicated in several pathologic conditions, such as schizophrenia (*2*), Parkinson disease (*3*), and addiction (*4*). Dopamine receptors are classified into 5 subtypes, D_1, D_2, D_3, D_4, and D_5 (*5*). The dopamine D_2 receptor is a main therapeutic target for currently used antipsychotic drugs and has long been suggested to be involved in the pathophysiology of schizophrenia (*2,6–11*).

Several observations in vitro indicate that the dopamine D_2 receptor exists in 2 interconvertible affinity states, distinguished by the affinity of endogenous dopamine and referred to as the high- and low-affinity states. It has further been suggested that the high-affinity state is the functionally active form of the receptor and is thus more relevant for clinical studies (*12*). Studies of dopamine D_2 receptors using PET have almost exclusively been performed with antagonist radioligands, such as ^{11}C-raclopride and ^{11}C-FLB457 (*13–15*). Antagonist radioligands do, however, bind with equal affinity to the 2 conformational states of the dopamine D_2 receptor. To examine the high-affinity state of the dopamine D_2 receptor in vitro and in vivo, agonist radioligands such as (−)-*N*-^{11}C-propyl-norapomorphine

Received Sep. 25, 2008; revision accepted Jan. 21, 2009.
For correspondence or reprints contact: Hiroshi Ito, Molecular Neuroimaging Group, Molecular Imaging Center, National Institute of Radiological Sciences 4-9-1, Anagawa, Inage-ku, Chiba, 263-8555, Japan.
E-mail: hito@nirs.go.jp

(^{11}C-NPA) and ^{11}C-(+)-4-propyl-3,4,4a,5,6,10b-hexahydro-2H-naphtho[1,2-b][1,4]oxazin-9-ol (^{11}C-PHNO) have recently been developed (*16,17*).

^{11}C-(*R*)-2-CH_3O-*N*-n-propylnorapomorphine (^{11}C-MNPA) is another new agonist PET radioligand with high affinity and selectivity for the dopamine D_2 receptor (inhibitory concentration of 50%, 1.02 nM; inhibition constant 0.17 nM, respectively) (*18,19*) and was recently characterized in nonhuman primates (*20*). PET measurements in cynomolgus monkeys showed high uptake in the striatum, with a striatum-to-cerebellum ratio of 2:2. The striatal uptake of ^{11}C-MNPA could be inhibited by the injection of unlabeled raclopride, confirming that the striatal binding is reversible and specific for dopamine D_2 receptors. Subsequent applied studies using amphetamine-induced dopamine release showed that ^{11}C-MNPA was more sensitive than ^{11}C-raclopride, thus supporting the indication that ^{11}C-MNPA is a promising radioligand for PET of the high-affinity state of the dopamine D_2 receptor in vivo (*21*). The aim of the present study was to examine the regional distribution and kinetics of ^{11}C-MNPA in the human brain. Ten control subjects were included, and data were analyzed using kinetic compartment analyses with a metabolite-corrected input function and 2 quantitative methods with the cerebellum as a reference brain region.

MATERIALS AND METHODS

Subjects

Ten healthy men (age range, 22–35 y; mean ± SD, 27.7 ± 5.4y) participated in this study. On the basis of their medical history and MRI of the brain, all subjects were free of any somatic, neurologic, or psychiatric disorders, and they had no history of current or previous drug abuse. Written informed consent was obtained from all subjects after the study was completely described. The study was approved by the Ethics and Radiation Safety Committee of the National Institute of Radiological Sciences, Chiba, Japan.

PET Procedure

^{11}C-MNPA was synthesized as described in detail previously (*20*). In brief, ^{11}C-MNPA was synthesized by the methylation of (*R*)-(−)-2,10,11-trihydroxy-*N*-n-propylnoraporphine-acetonide with ^{11}C-methyl triflate and subsequent cleavage of the acetonide protecting group with the addition of hydrochloric acid. An ECAT EXACT HR+ PET system (CTI-Siemens) was used for all measurements. A head-fixation device was used to minimize head movements during data acquisition. A transmission scan for attenuation correction was obtained using a ^{68}Ge–^{68}Ga source. Dynamic PET scans were obtained after a 1-min intravenous slow bolus injection of ^{11}C-MNPA (204.3–232.1 MBq; mean ± SD, 219.3 ± 8.2 MBq). The specific radioactivity of ^{11}C-MNPA was 197.5–335.0 GBq/μmol (261.1 ± 43.3 GBq/μmol) at the time of injection. Brain radioactivity was measured from 0 to 90 min (20 s × 9, 1 min × 5, 2 min × 4, 4 min × 11, and 5 min × 6).

MR images of the brain were acquired with a 1.5-T MRI scanner (Gyroscan NT; Philips). T1-weighted images were obtained at 1-mm slices acquired in 3 dimensions.

Arterial Blood Sampling and Metabolite Analysis

To obtain the arterial input function, a series of arterial blood samples were taken manually from a catheter 32 times (2.5 mL × 22 times for the measurement of radioactivity concentration in whole blood and plasma; 5.0 mL × 10 times for the determination of the percentage of unchanged ^{11}C-MNPA in plasma) during the 90-min PET scan. Each blood sample was centrifuged to obtain plasma and blood cell fractions, and the concentrations of radioactivity in whole blood and plasma were measured.

The percentage of unchanged ^{11}C-MNPA in plasma was determined by high-performance liquid chromatography (HPLC) in 10 of the blood samples. Acetonitrile was added to each plasma sample, and the samples were then centrifuged. The supernatant was subjected to radio-HPLC analysis (column, XBridge Prep C18; Waters) (mobile phase, 48:52 90% acetonitrile:50 mM ammonium acetate). The arterial plasma input function was defined as the radioactivity of plasma multiplied by the percentage of unchanged radioligand.

Regions of Interest (ROIs)

All MR images were coregistered to the PET images using the statistical parametric mapping system (SPM2; Wellcome Trust Centre for Neuroimaging) (*22*). ROIs were drawn manually on summated PET images with reference to the coregistered MR images. ROIs were defined for the cerebellar cortex, putamen, caudate, and thalamus. Regional radioactivity was calculated for each frame, corrected for decay, and plotted versus time.

Kinetic Compartment Analysis of ^{11}C-MNPA Binding

To describe the kinetics of ^{11}C-MNPA in the brain, the 2-tissue-compartment model with 4 rate constants, K_1, k_2, k_3, and k_4, was used. The 3 compartments include C_P, the radioactivity concentration of unchanged radioligand in plasma (arterial input function); C_{ND}, the radioactivity concentration of nondisplaceable radioligand in the brain (including nonspecifically bound and free radioligand); and C_S, the radioactivity concentration of radioligand specifically bound to receptors. The rate constants K_1 and k_2 represent the influx and efflux rates for radioligand diffusion across the blood–brain barrier. The rate constants k_3 and k_4 represent radioligand transfer between the compartments for nondisplaceable and specifically bound radioligand.

Calculation of the ^{11}C-MNPA Binding Potential

^{11}C-MNPA binding was expressed by the indirect kinetic, SRTM, and transient equilibrium methods. In these methods, ^{11}C-MNPA bindings were expressed as binding relative to nondisplaceable binding (BP_{ND}) (*23*). The BP_{ND} of the radioligand is proportional to the product of the receptor density (B_{max}) and reciprocal affinity ($1/K_d$), and the ratio of B_{max} to K_d corresponds to the ratio of k_3 to k_4, as expressed by the following equation:

$$BP_{ND} = f_{ND}(B_{max}/K_d) = k_3/k_4, \qquad \text{Eq. 1}$$

where f_{ND} is the free fraction of radioligand in the nondisplaceable compartment. The cerebellum (cerebellar cortex) was used as a reference brain region because it is a structure with negligible D_2 dopamine receptor density (*24*). The software package PMOD (PMOD Technologies) was used for the indirect kinetic, SRTM, and transient equilibrium quantitative methods.

Indirect Kinetic Method. In the present cross-validation approach, the indirect kinetic method was used as the standard method (*25*). BP_{ND} was defined as the ratio of k_3 to k_4 as calculated using the 2-tissue-compartment model. Because the ratio of k_3 to k_4 is sensitive for noise in the PET data, BP_{ND} was

calculated using the indirect kinetic method. With the cerebellum as a reference region, BP_{ND} can be expressed as:

$$BP_{ND} = V_{T(region)}/V_{T(cerebellum)} - 1, \quad \text{Eq. 2}$$

where $V_{T(region)}$ is the total distribution volume ($= (K_1/k_2)(k_3/k_4 + 1)$) in a target region, and $V_{T(cerebellum)}$ is the total distribution volume ($= K_1/k_2$) in the cerebellum. The rate constants K_1, k_2, k_3, and k_4 in the putamen, caudate, and thalamus were determined by nonlinear curve fitting in a least-squares sense to the regional time–activity curves as described in the literature (*15*). K_1 and k_2 values in the cerebellum were also determined by nonlinear curve fitting in a least-squares sense but by using the 1-tissue-compartment model, assuming that the cerebellum has negligible D_2 dopamine receptor density (*24*). To improve the stability of the curve fitting in the nonlinear curve-fitting procedure, the ratio of K_1 to k_2 was fixed for each subject to the value obtained in the cerebellum by the kinetic analysis with the 1-tissue-compartment model (range of K_1/k_2, 5.0–7.9 mL/cm^3; mean ± SD, 6.5 ± 0.75 mL/cm^3). In this analysis, blood volume, which depends on the first-pass extraction fraction of the tracer, was estimated using the radioactivity of whole blood to diminish the influence of tracer remaining in the blood (*26*).

SRTM Method. The SRTM method, assuming that both target and reference regions have the same level of nondisplaceable binding, can be used to interpret time–activity curves in the target region as follows (*27*):

$$C_T(t) = R_1C_R(t) + (k_2 - R_1k_2/(1+BP_{ND}))C_R(t) * \exp(-k_2t/(1+BP_{ND})), \quad \text{Eq. 3}$$

where $C_T(t)$ is the total radioactivity concentration in a brain region measured by PET, R_1 is the ratio of K_1 to K_1' (K_1, influx rate constant for the brain region; K_1', influx rate constant for the reference region), $C_R(t)$ is the radioactivity concentration in the reference region (cerebellum), and * denotes the convolution integral. The parameters R_1, k_2, and BP_{ND} in this model were estimated by the nonlinear curve-fitting procedure.

Transient Equilibrium Method. Transient equilibrium theoretically occurs when the derivative for specific binding ($dC_S(t)/dt$) is 0, that is, the peak point of specific binding, $C_S(t)$ (*15,28*). It follows that $C_S(t)/C_{ND}(t)$ is equal to k_3/k_4 ($= BP_{ND}$) at transient equilibrium.

Simulation Study

A simulation study was performed to estimate errors of BP_{ND} calculated by the SRTM and transient equilibrium methods. The assumed values and intervals examined were acquired from the results of the kinetic approach. Regional tissue time–activity curves (0–90 min) were generated according to the 2-tissue-compartment model. We assumed that the value of K_1/k_2 equaled 6.6 mL/cm^3 and that of k_4 equaled 0.18 min^{-1}. The tissue time–activity curves were generated with K_1 values between 0.20 and 0.60 mL/cm^3/min in 6 steps and with k_3 values between 0.02 and 0.20 min^{-1} in 10 steps. A tissue time–activity curve for the cerebellum was generated according to the 1-tissue-compartment model with 2 rate constants, using 0.44 mL/cm^3/min for K_1 and 0.067 min^{-1} for k_2. The average arterial input function ($n = 10$), corrected for labeled metabolites, was used to generate the tissue time–activity curves. BP_{ND} was then calculated by applying the SRTM and transient equilibrium methods to the generated tissue time–activity curves. The estimated BP_{ND} values were compared with the BP_{ND} values calculated by the indirect kinetic method.

Variations in K_1 values between a brain region and the cerebellum due to differences in cerebral blood flow (CBF) between

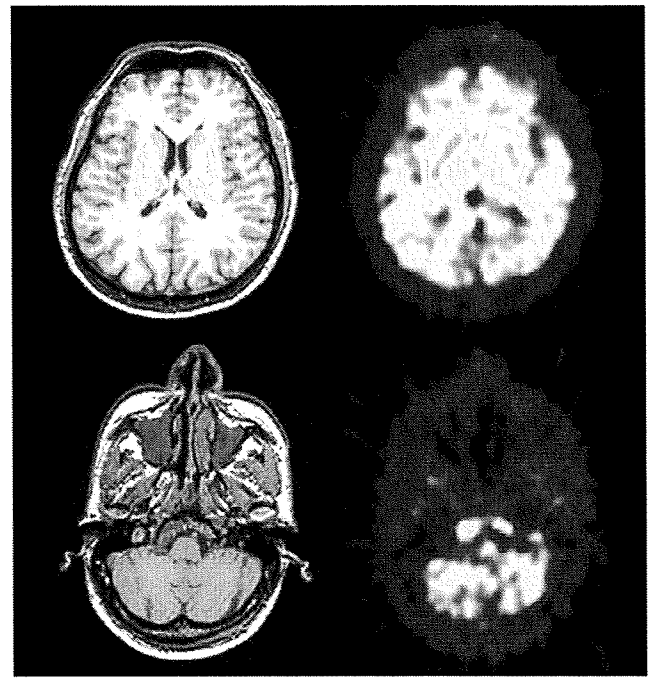

RGB

FIGURE 1. Representative summated PET images 60–90 min after intravenous injection of ^{11}C-MNPA (221 MBq) and corresponding T1-weighted MR images in control human subject. Upper panel shows horizontal section through striatum, and lower panel shows section through cerebellum.

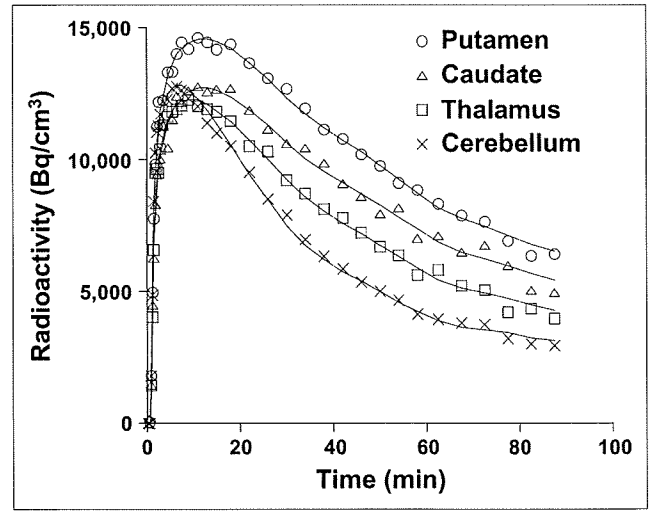

FIGURE 2. Representative regional time–activity curves after intravenous injection of ^{11}C-MNPA (232 MBq) binding in control human subject. Fitted curves using 2-tissue- and 1-tissue-compartment models are also shown for target regions and cerebellum, respectively.